Study on structure-property relationship of 1,5-naphthyridine-2,6-dione (NTD) derivatives for organic field-effect transistors

유기 전계 효과 트랜지스터를 위한 1,5-Naphthyridine-2,6-dione (NTD) 유도체의 구조 – 성질에 관한 연구

2019년 8월

서울대학교 대학원

재료공학부

리우메이린

Study on structure-property relationship of 1,5-naphthyridine-2,6-dione (NTD) derivatives for organic field-effect transistors

유기 전계 효과 트랜지스터를 위한 1,5-Naphthyridine-2,6-dione (NTD) 유도체의 구조 – 성질에 관한 연구

지도교수 박 수 영

이 논문을 공학석사학위논문으로 제출함

2019년 8월

서울대학교 대학원

재료공학부

리 우 메 이 린

리 우 메 이 린의 공학석사학위 논문을 인준함

2019년 8월

위 원 장   서용석   (인)

부위원장   박수영   (인)

위   원   김재필   (인)

Study on structure-property relationship of 1,5-naphthyridine-2,6-dione (NTD) derivatives for organic field-effect transistors

A THESIS SUBMITTED IN PARTIAL FULFILLMENT OF
THE REQUESTIMENTS FOR THE DEGREE OF
MASTER IN ENGINEERING AT THE GRADUATE
SCHOOL OF SEOUL NATIONAL UNIVERSITY

AUGUST 2019

By

Meilin Liu

Supervisor

Prof. Soo Young Park

Abstract

Study on structure-property relationship of 1,5-naphthyridine-2,6-dione (NTD) derivatives for organic field-effect transistors

Meilin Liu

Department of Materials Science and Engineering

The Graduate School

Seoul National University

Organic field-effect transistors (OFETs) have attracted great attention due to their advantages of flexibility and solution processability. Many researchers have made great efforts on development of high-performance organic semiconductor materials and exploring their structure-property relationships to optimize the device performances. Among many organic semiconductors, organic molecules containing bis-lactam functional groups have been drawing special attention for high-performance OFET materials because of their high electron affinity, tunable solubility, and strong π-π interaction.

Recently, a novel bis-lactam-based small molecule, 1,5-dioctyl-3,7-di(thiophene-2-yl)-1,5-naphthyridine-2,6-dione (NTDT), was developed. In comparison with the well-known bis-lactam-based semiconducting material such as 2,5-dioctyl-3,6-di(thiophen-2-yl) pyrrolo[3,4-c]pyrrole-1,4-dione (DPPT), NTDT exhibited more favorable thin-film morphology and electronic coupling structures for charge transport due to two-dimensional (2D) C-H···O=C intermolecular interaction, highly planar molecular structure, and strong intermolecular π–π stacking. Although NTDT showed promising hole mobility in the OFET

devices, there is still much room for further improvement. Therefore, studying structure-property relationships of NTDT derivatives is highly desired.

This study aims to investigate the effect of molecular planarity and crystallinity on the performance of OFET devices using NTDT-based semiconductors. In this work, we designed and synthesized a series of NTDT derivatives bearing additional two hexyl side chains at three different positions (α, β, and γ) in the thiophene rings of NTDT. Their optoelectronic properties were thoroughly investigated by UV-vis absorption, photoluminescence, and cyclic voltammetry (CV) measurements as well as theoretical calculation using density functional theory (DFT) method. It was found that the substitution position of the hexyl chains influenced molecular planarity of the NTDT derivatives, which significantly altered their optoelectronic and thermal properties as well as crystallinity in the solid state. Interestingly, the photoluminescence quantum yields (Φ_{PL}) of the NTDT series were unity in solution state regardless of the substitution of additional hexyl chains. In contrast, in films, the NTDT derivatives showed different Φ_{PL} values depending on the substitution position of the hexyl chains.

Finally, vapor-deposited and solution-processed OFET devices were fabricated using the NTDT derivatives. In the vapor deposited devices, Octyl-NTDT-αhexyl showed the best hole mobility (μ_h) up to 0.44 $cm^2 V^{-1} s^{-1}$ among the series, while Octyl-NTDT-βhexyl showed the best μ_h as high as $9.11 \times 10^{-2} cm^2 V^{-1} s^{-1}$ in the solution-processed devices. In contrast, the μ_h of Octyl-NTDT-γhexyl was significantly low in both devices due to the twisted molecular structure. Through X-ray diffraction (XRD) studies, it was revealed that there was a correlation between the substitution position, crystallinity, and device performance of the NTDT derivatives.

Keywords:1,5-naphthyridine-2,6-dione, Small molecule, D-A structure, Structure-Property Relationship, Organic Field-Effect Transistor.

Student Number:2017-21750

Contents

List of Tables

List of Schemes

List of Figures

x

Chapter 1. Introduction

1.1 Organic Field-Effect Transistors (OFETs)

1.1.1 Introduction of OFETs

Field effect transistor (FET) is thought to function as an electronic device that amplifies and converts electrical signals. In 1947, the first practical device was manufactured by John Bardeen, William Shockley and Walter Brattain at Bell Laboratory. Compared with the electron tubes, transistors are smaller in size and lower power consumption. A prodigious development of electronic technology was achieved by the advent of transistor made and these three scientists have won the Noble Prize for Physics in 1956.

Initially, traditional transistors are generally based on inorganic semiconductors such as silicon, germanium and III-V compounds. In the 1980s, researchers began to introduce conjugated polymers and small molecules as active layer materials into field effect transistors and prepare organic field effect transistors. In 1986, Tsumura et al. first reported the OFET using polythiophene as an organic semiconductor layer, and the carrier mobility of it was 10^{-5} cm^2 V^{-1} s^{-1}, and the switching ratio was 10^2-10^3, it also shows the advantages of organic field effect transistors in low cost and large area production. [7] Although the performance of organic devices is far behind that of inorganic materials, it has triggered a wave of research on it. Since then, it has been developed rapidly and the performance of devices has been improved continuously. High-performance field effect transistor is one of the essential components in state-of-the-art applications such as display drivers, radio-frequency identification (RFID) tags, [1] amplifiers, and analog-to-digital and digital-to-analog converters, [8] organic integrated circuits and display. [9] And now, the state of art charge carrier mobility of p-type organic thin film field effect transistor has more than 40 cm^2 V^{-1} s^{-1} for hole mobility, [10] and 11 cm^2 V^{-1} s^{-1} for electron mobility. [11] More and more organic semiconductors have been proven to have excessive mobility and superior performance than traditional amorphous silicon devices. Compared with traditional

inorganic semiconductors, organic semiconductor devices are expected to have a series of advantages such as large area, flexible, low cost and easy processing, which is favorable to be applied to flexible circuits, sensors, flexible display panels, lasers and other fields. [12] In addition, the performance of the device could be controlled by changing the structure of the organic semiconductor, and appropriative structure of organic semiconductor material could also be designed according to the requirements of the device. Therefore, the research on organic semiconductor devices has attracted a large number of researchers in recent years.

1.1.2 Operational principle of OFETs

According to the device structure, OFET can be divided into four types: Bottom-gate bottom-contact (BGBC), Top-gate bottom-contact (TGBC), Bottom-gate top-contact (BGTC) and Top-gate top-contact (TGTC) **(Figure 1. 1)**. [13] Device structure plays a significant impact on device performance. [14] As Chong-an Di et al point out, the device structure with bottom-gate top contact and top-gate bottom contact has better performance due to the source and drain electrodes have better contact with organic semiconductors and lower contact resistance. which arising from large injection areas and favored injection paths compared with BGBC and TGTC devices. [13] Nevertheless, the most critical factor affecting OFET is the organic semiconductor layer. such as the molecular stacking of organic semiconductor materials, [15] the frontier orbital level, [16] the contact resistance [17] with metal electrodes and the organic/electrode interface effect, [18] which all affect the charge mobility of the device.
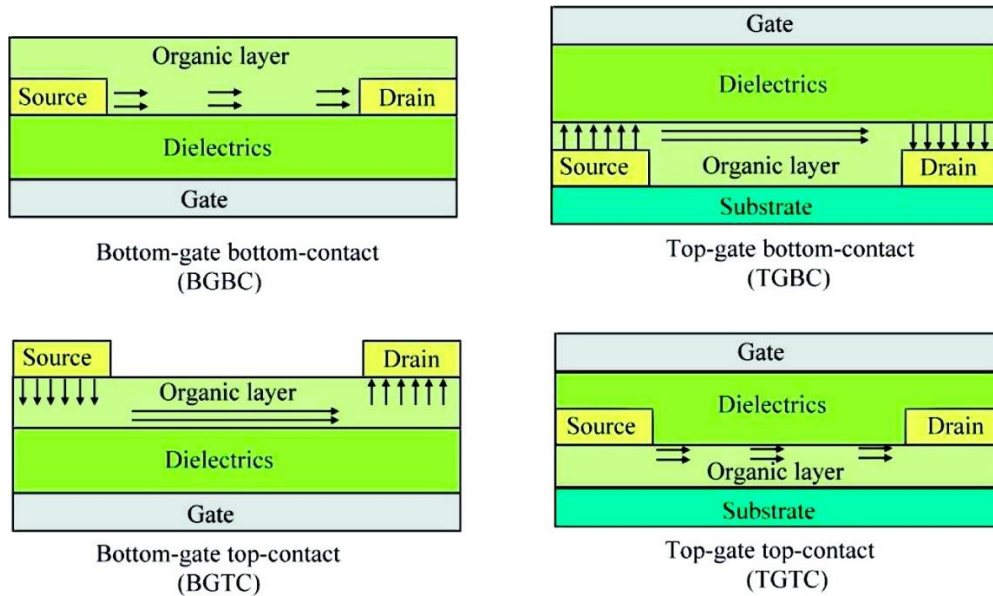
Figure 1. 1 Architectures of OFET devices (a) Bottom-gate bottom-contact (BGBC), (b) Top-gate bottom-contact (TGBC), (c) Bottom-gate top-contact (BGTC) and (d) Top-gate top-contact (TGTC) bottomcontact configuration. [13]

The operation principle of organic field effect transistor is that the conductive channel is formed at the interface between semiconductor layer and insulating layer by applying external electric field. The device consists of three electrodes, that is, source, drain and gate.[19] The gate voltage (V_G) applied between the gate and the source could generate an electric field, which causes the charge accumulation at the interface between the insulating layer and the semiconductor layer, thereby the source-drain current (I_{DS}) flowing in the semiconductor material can be regulated. [20] If no gate voltage is applied between the gate and the source ("off state"), the device acts as a resistor since the resistance of the organic semiconductor material is large and there is almost no current passing between the source and drain electrodes. [21] When a negative or positive V_G is applied, positive charge (hole) or negative charge (electron) could be injected from the source electrode and accumulated at the interface between the semiconductor layer and the insulating layer, which is referred to as the "on state" **(Figure 1. 2)**. [22] The amount of accumulated charge is proportional to the V_G and the capacitance C_i of the insulator. But, there have been reports where not all the induced charges are mobile and will contribute to the current in the organic field effect transistor. The trap must be filled before the additional induced charge can be moved. In other words, a gate voltage applied needs to be higher than the threshold voltage V_{Th}, so the effective gate voltage is V_G-V_{Th}. [23a,23b,23c]
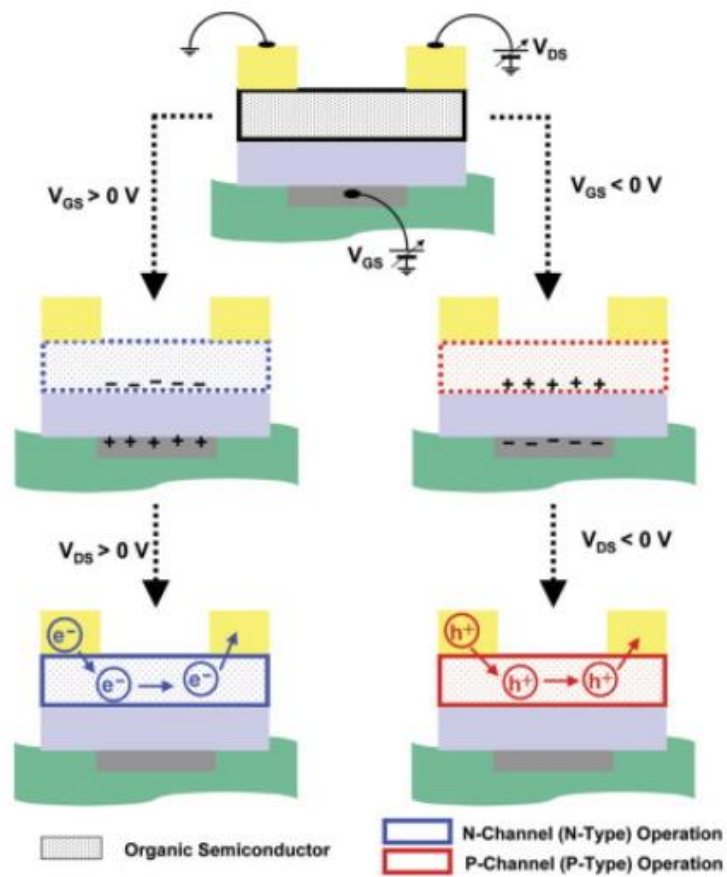
Figure 1. 2 Transistor operation of p- and n-channel thin-film. [22]

Considering from the aspect of energy level, in this situation, if the HOMO or LUMO energy levels of semiconductor materials is close to the Fermi level (E_f) of the source and drain metal electrodes, the charge carriers will be injected and extracted respectively, resulting in the generation of current flow. Since the current value increases with the increasing of the V_G until a saturation value is reached, and the slight change of the voltage causes a large change of the current, the effect of the signal amplification of the OFETs can be achieved. [24] In general, the working principle of OFETs is shown in the following **Figure 1. 2**. When transistors are at "off state", the gate bias is zero, the position of HOMO and LUMO levels can be seen from **Figure 1. 3**, which is shifted with the E_f. With positive V_G being applied, the LUMO and HOMO levels would be shifted down in relative to the Fermi level. And the LUMO level could be resonant with E_f of contact under a large gate voltage and the electrons can flow from the contact to the LUMO of semiconductor, resulted in the current flow from source and drain, which is applied for the n-type transistor. If the negative gate bias was applied, negative gate voltage raises the orbital up, possibly making the alignment of HOMO energy level closer to E_f, thus resulting in the hole transport , which is referred to the p-type transistors. Consequently, when a gate voltage is applied, the HOMO and LUMO energy levels will be aligned with the E_f, then the electron or holes would flow from the metal to the energy orbital **(Figure 1. 3).** [12]
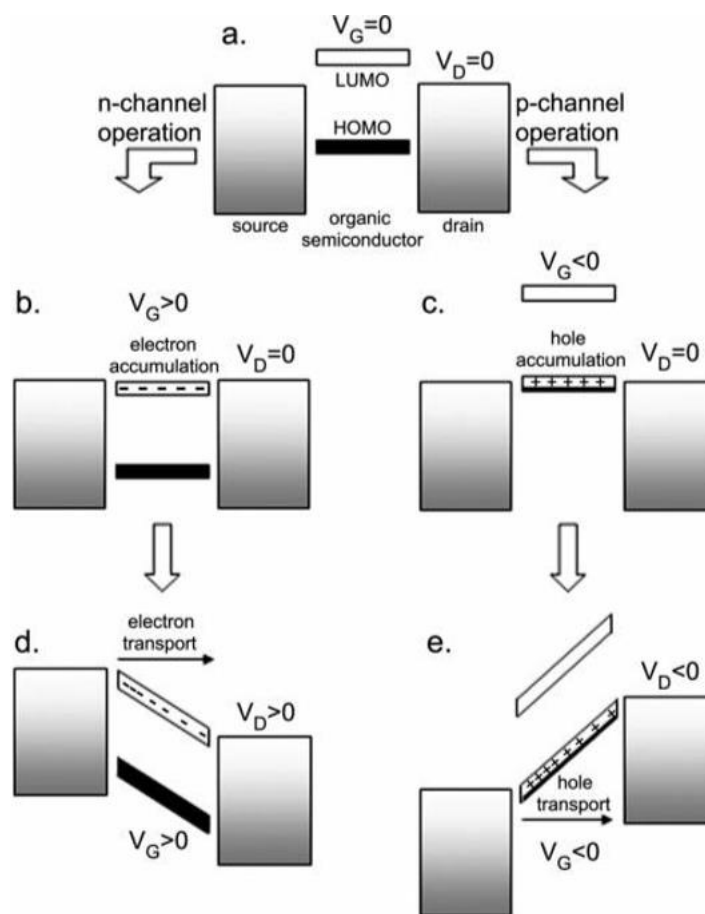
Figure 1. 3 Schematic representation of the HOMO and LUMO of the organic semiconductor with respect to the source-drain metal Fermi level. [12]

In general, for p-type transistor, when a negative V_G is applied, holes are injected into the organic semiconductor layer from the source and accumulated at the interface between the organic semiconductor and the insulating layer, then a negative voltage V_{DS} is added between the source and the drain, the current flow (I_{DS}) can be generated between source and drain and modulated by the magnitude of both the gate voltage (V_G) and the drain-source voltage (V_{DS}). [25] The carrier density in the conductive channel is uniform with no V_D being applied during the "off state" **(Figure 1. 4 (b))**. [23a] But under the applied source-drain voltage (V_{DS}), there is a driving force to make accumulated charge carriers from the source to drain electrode where drain current (I_{DS}) can be modulated by the gate voltage. The electric field intensity is regulated by gate voltage and the carrier density varies with the change of electric field intensity finally resulting in the change of drain current (I_{DS}) between the source and drain electrodes, which strongly suggests that the current density and the current can be modulated by the magnitude of the field applied. [26] This is referred to as the "field effect".

1.1.3 Device characterization

Figure 1. 4 (a) shows the drain current versus increasingly negative drain voltage where each curve is measured at a fixed gate voltage, which is known as "output curve". From the output curve, the linear and saturation regimes can be observed. For the P-type transistors, when the source-drain voltage is small, $V_{DS} \gg V_G\text{-}V_{Th}$, the device is in the linear regime, where the drain current exhibited good linearity, which accorded with Ohm's law and is proportional to gate voltage and drain voltage. **(Figure 1. 4 (b))**. And the drain current I_D can be approximately expressed as equation 1.

$$I_{DS,lin.} = \frac{W}{L}\mu_{lin.}\mathbf{C}_i(V_G-V_{Th})V_{DS} \qquad (1)$$

where C_i is the capacitance per unit area of the insulating layer, W is the channel width, L is the channel length, and μ is the field effect charge mobility. [26]

For a certain gate voltage, when the source-drain voltage continued to increase, with the gradual increase of drain voltage, difference between source-drain voltage and gate voltage have become smaller,a point $V_{DS} = V_G - V_{Th}$ is reached near the drain electrode, at which the free charge carriers are depleted and the channel is "pinched off". [26,27] Under the applied electric field, space charge limited saturation $I_{DS,sat}$ current flows across the narrow depletion zone from pinch-off point to the drain. **(Figure 1. 4 (c))**. [23,26] Then, with further increasing source-drain voltage, the saturation current will no longer increase as the drain voltage increases but lead to the expansion of the depletion zone near the drain, resulting in a slight shortening of the channel. **(Figure 1. 4 (d))**

The current in the saturation region is given by equation 2.

$$I_{DS,sat.} = \frac{W}{2L}\mu_{sat.}\mathbf{C}_i(V_G - V_{Th})^2 \qquad (2)$$

Here, mobility can be measured in the saturated region:

$$\mu_{sat.(VG)} = \frac{\partial I_{DS,sat}}{\partial V_G} \cdot \frac{L}{WC_i} \frac{1}{V_G - V_T} \qquad (3)$$

Mobility (μ), a measure of how quickly carriers move in the semiconductor layer in response to the electric field, is the most critical factor used to measure the performance of an organic field effect transistor that can be determined from the slope of the linear plots of $(I_{DS,sat.})^{1/2}$ versus V_G. The larger the value, the better the device performance, indicating the

average value of the transport speed of the charge carriers in the electric field intensity per unit equivalent. The mobility is calculated from the slope of the linear regime in **Figure 1. 5 (a)** in red line, $\frac{\partial I_D}{\partial V_G}$,, and from the slope of the saturation regime with the red line in **Figure 1. 5 (b)**, $\frac{\partial \sqrt{I_D}}{\partial V_{GS}}$, respectively. [26]

Also，from **Figure 1. 5 (a)** and **Figure 1. 5 (b)**, drain current in the linear regime can be obtained from the blue line, and Figure 3b indicates the square root of the drain current. In black, **Figures 1. 5 (a)** and **1. 5 (b)** show the drain current on a logarithmic scale as a function of gate-source voltage at a fixed source-drain voltage in the linear and saturation regimes respectively. [26]
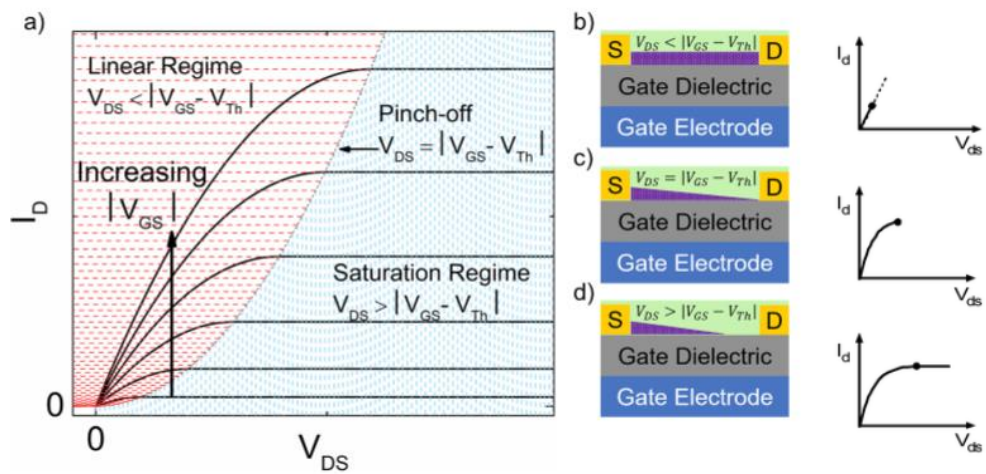
Figure 1. 4 (a) Ideal OFET output characteristics, (b)–(d) BGBC architectures of OFET devices (b) in the linear regime, (c) at pinch-off, and (d) in the saturation regime. [26]
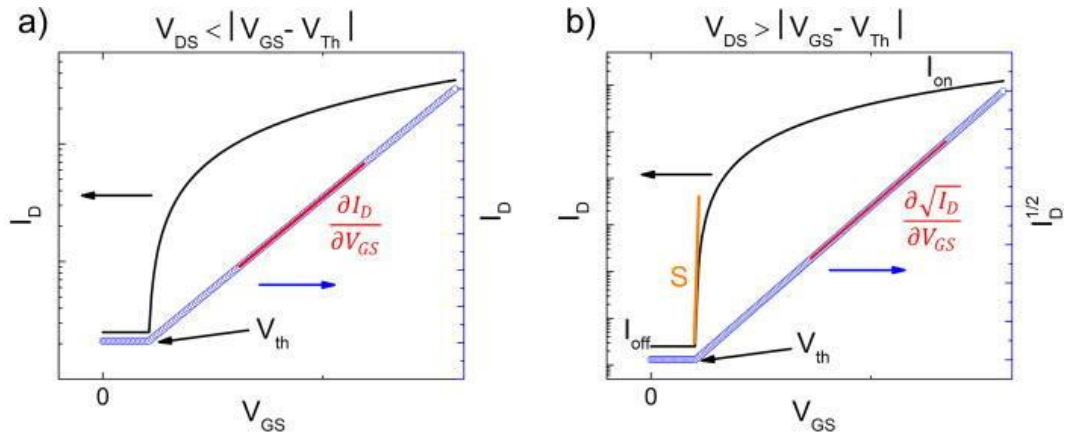
Figure 1. 5 Changes of I_D at fixed, negative, V_{DS} with the increase of V_{GS} in (a) the linear regime and (b) the saturation regime. [26]

In order to depict the device characterization, output curve and transfer curve are essential. The output curve is to keep V_G unchanged, and I_{DS} is plotted against V_{DS}. The transfer curve is to maintain V_{DS} unchanged, and I_{DS} is plotted against V_G. **(Figure 1. 6)**

For evaluation of the performance of organic field-effect transistor devices, there are many factors used to measure the performance of organic field effect transistors such as mobility (μ), current ratio ($\frac{I_{on}}{I_{off}}$), and threshold voltage (V_{Th}). The most critical parameter is the mobility of the carrier because it represents the operating frequency and power of the device. The parameters that can have an influence on the value of μ mainly include: the purity of the organic compound, [28,29] the contact at the interface, [30] the modification of the surface of the insulating layer, [31] and so forth. Current ratio ($\frac{I_{on}}{I_{off}}$), the ratio of source-drain current when the transistor is in the "on" and "off" state within a certain V_G range, is another one that can impact performance that determines the switching performance from the off to the on state of the transistor. Generally, the more stable the field effect transistor is, the larger the current ratio is. Also, the threshold voltage (V_{Th}) is the lowest voltage required to turn on a device, representing the power dissipation of the transistor. So, the lower the threshold voltage, the smaller the power consumption of the transistor. Not only organic semiconductor active layer but the gate dielectric materials greatly affect the device performance. [25,32]
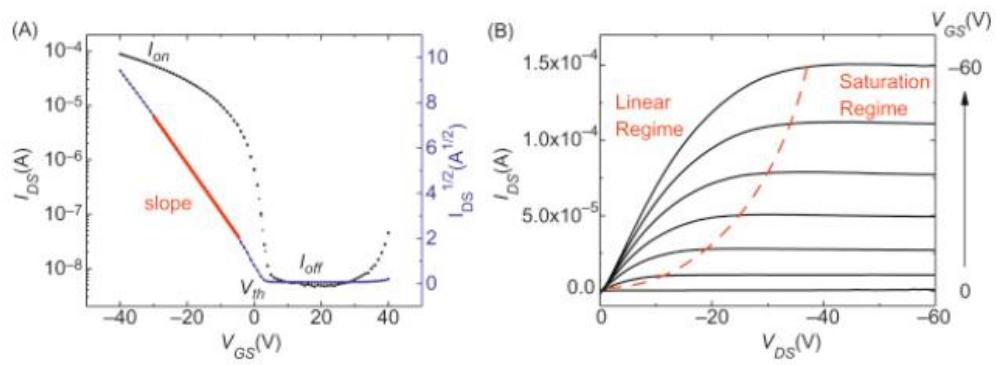
Figure 1. 6 P-type FET transistor characteristics: (A) transfer and (B) output curves.

1.1.4 Organic semiconductors for OFETs

From the material aspect, as an active layer material in organic thin film transistors, organic semiconductor materials have a significant role in determining the performance of organic thin film transistor devices. And the intrinsic properties of semiconductor materials determine the type and transport characteristics of carriers. So far, great achievements have been made in the field of preparation of novel organic thin film transistor devices using solution process technology with good air stability.

The organic small molecule semiconductors have attracted many researchers' attention due to its advantages such as well-defined structure, simple purification, high performance, and easy preparation of a single crystal structure. However, the development has some inherent limitation because of its strict preparation conditions, poor processing performance, susceptible to outside interference and poor stability. The performance of semiconductor materials is mainly determined by two impressive factors: intramolecular and intermolecular charge transport. Electronic delocalization area and planarity structure are the most favorable controlling factors for intramolecular charge transport in semiconductors. Delocalization is a critical feature of molecular orbital theory where electrons can exist in molecular orbitals that are spread over the entire molecule. The delocalization of HOMO and LUMO orbitals is expected to be more uniform in the entire molecular skeleton, which resulted in better intramolecular charge carrier transport. And rigid conjugated backbone is also an important feature of semiconductors for OFET, it can form large conjugated π electron system so that the charge can transfer within the molecule.

Also, the introduction of heteroatoms such as sulfur and nitrogen caused more planar molecular skeletons due to noncovalent interaction (S…π, S…C, or N-H…π, etc.). [33a] And Intermolecular charge transport should be attributed to intermolecular distance, molecular packing orientation, degree of π-stacking overlap. As Shi et al point out, a reasonable adjustment in the π-stacking characteristics of organic semiconductors will give rise to a large transfer integral and hence fine transport properties. [33b] To date, numerous of studies had been made about π-conjugated small molecules because of their advantages, hole mobility of p-type organic thin film field effect transistor has more than 40 $cm^2 V^{-1} s^{-1}$, [10]

and 11 $cm^2 V^{-1} s^{-1}$ for electron mobility was achieved. [11]

1.1.4.1 P-type organic semiconductors

P-type organic semiconductor involving π-conjugation and deep HOMO levels is considered as an excellent hole transport material which has the exact effect on electron-donating properties and air stability. In general, HOMO level is recommended to be in the range of -5.0 to -5.5eV, which is appropriate for the work function of gold electrode ($W_f =$ 5.1 eV). [34] And now, many organic semiconductors showing p-type FET characteristics have been reported such as pentacene, acenes and heterocyclic oligomers, that exhibit higher hole mobilities than amorphous Si (～1.0 $cm^2 V^{-1} s^{-1}$). The typical p-type small molecule organic field effect materials mainly are fused ring aromatic hydrocarbons as well as derivatives and heterocycles and their derivatives.

The most commonly used structural unit in the π-conjugated system is the benzene ring because of the uniform distribution of π electrons within the benzene ring molecule, which forms a strong interaction force between the molecules, thus forming ordered and closing molecular packing in solid-state which is more suitable for the hole transport. And pentacene (1) with HOMO level of -5.14 eV is relatively easy to transport holes and shows the highest mobility (μ) value of 3.0 $cm^2 V^{-1} s^{-1}$. [35a] In 2004, Oana D. Jurchescu et al developed a single crystal transistor using pentacene with reduced impurity concentration of pentacenequinone by a pretreatment consisting of vacuum sublimation of the impurity under a temperature gradient and mobility of 40 $cm^2 V^{-1} s^{-1}$ was achieved. [35b] Although the mobility of pentacene-based devices has been greatly improved, it has some disadvantages of poor stability and poor solubility, which is not conducive to separation and purification, and even more difficult to prepare for thin film devices. Therefore, in order to increase the solubility issue of pentacene, scientists began to improve the structural composition of pentacene. In 2001, the Anthony group introduced a large sterically hindered TIPS at the 6 and 13 active sites of pentacene to obtain compound 8, which has good solubility and is stable in air. [35c] As is reported, introducing triisopropylsilylethynyl to pencene has significant effects on the change of packing style from herringbone to brick layer in

pentacene and TIPS-pentacene, which might be caused by the steric effect of side chains. Therefore, the side chains do not only improve the solubility, but also that help to force the conjugated rings to stack with π–π orbital overlaps as auxiliary groups. [35d] The properties of picene (2) that is an isomer of pentacene are differed greatly from those of pentacene (1), its oxidation stability is higher than pentacene due to picene has an energy level of 3.3 eV and an ionization potential of -5.5 eV. The Okamoto group developed a picene-based thin film FET with mobility of 1.1 $cm^2 V^{-1} s^{-1}$ and a switching current ratio of 10^5, performance of which was improved by exposure to air or O_2 for a long time. [35e] Rubrene (15) is a derivative of tetracene. The introduction of four phenyl groups increases the π...π interaction, and the optimized mobility of single crystal FET is as high as 14 $cm^2 V^{-1} s^{-1}$. The μ value of 40 $cm^2 V^{-1} s^{-1}$ was achieved. [35f]

As another example, introducing the thiophene ring into pentacene is feasible to control intermolecular force, and it proves to be feasible. Since there is a pair of lone pairs of electrons on the sulfur atom, the thiophene has a higher charge density than the benzene ring, which is beneficial to control the electron distribution orbit of the molecule, lowering the energy level of the molecule and increasing the band gap of the molecule. Therefore, replacing the benzene rings of pentacene with thiophene rings is also becoming a research hotspot for its significant benefit of enhancing environmental stability, intermolecular force, etc. [35g] Mobility of thiophene-containing compound (3) with linear conjugated structure has been reported to achieve 0.47 $cm^2 V^{-1} s^{-1}$ and low threshold voltage (7 V). [35h]

Since then, more research around the fused-thiophene has been carried out, Liu Yunqi's group synthesized pentathienoacene (4) with a lower HOMO level (HOMO = -5.33 eV) than pentacene and then prepared thin film device by vacuum deposited and the μ value of the device was 0.05 $cm^2 V^{-1} s^{-1}$. [35i] Subsequently, hexathienoacene (6) was synthesized by Yu et al. The higher molecular order was formed due to the extended π-conjugation length and planarity molecular structure so that the highest μ value of 0.006 $cm^2 V^{-1} s^{-1}$ was achieved. [35j] Further, the π-conjugated length was extended on the basis of pentathiophene, and compound (7) was prepared by Okamoto to prepare a single crystal device, and the μ was 0.5 $cm^2 V^{-1} s^{-1}$. [35k] In addition, Cn-BTBT (5) have attracted much attention from application due to the solubility of the alkyl-substituted compound is improved so that the organic semiconductor layer can be prepared by a spin-coating. When the alkyl chain is -

$C_{12}H_{25}$, the film device performance is 3.9 cm^2 V^{-1} s^{-1}, [36a] When the substituent is -$C_{13}H_{27}$, the highest hole mobility is 2.75 cm^2 V^{-1} s^{-1}. [36b] Continue to expand the π-conjugated system, the highest mobility of both DNTT (11) and DATT (10) is nearly 3.0 cm^2 V^{-1} s^{-1}. [37]

Aza-fused ring and its derivatives are generally realized by substituting the benzene ring of acene compounds with nitrogen heterocycles. The introduction of nitrogen atoms not only does not destroy the skeleton of the entire molecule and its planarity but also helps to reduce the HOMO level, increasing the stability in air. It is worth to note that introducing nitrogen atom facilitates the formation of the hydrogen bond that enables molecules to come into close packing, which is attributed to stronger intra- and intermolecular interactions resulting in relatively high transistor performance (high mobility is referred to ~0.1 cm^2 V^{-1}s^{-1}). A series of soluble carbazole derivatives (16) was prepared with the addition of the two nitrogen atoms on which various solubilizing groups can be added to enhance the solubility. [38a] They developed an OFET device based on the compound that was prepared by introducing the octylphenyl group to the nitrogen atom (16b). and the measured μ value was 0.12 cm^2 V^{-1} s^{-1}. After that, they reported that the substitution of the carbazole core with a phenyl unit (17) is an effective way to improve the performances, which can extend the π-conjugation length to improve molecular self-organization and molecular packing, leading to the increase of carrier transport. [38b] The mobility (μ) of the (17) thin film device was 0.2 cm^2 V^{-1} s^{-1}, and the mobility of 0.22 cm^2 V^{-1} s^{-1} at compound (18) was achieved due to the strong NH–π interaction between molecules. [39]

(1)

Pentacene 3 cm^2 V^{-1} s^{-1} [35b]

(2)

Picene 3 cm^2 V^{-1} s^{-1} [35e]

(3)

Tetraceno[2,3-b]thiophene
0.47 cm^2 V^{-1} s^{-1} [35h]

(4)

Pentathienoacene (PTA)
3 cm^2 V^{-1} s^{-1} [35i]

(5)

Picene Cn-BTBT
a R$_1$=C$_{12}$H$_{25}$ 3.9 cm^2 V^{-1} s^{-1} [36a]
b R$_2$=C$_{13}$H$_{27}$ 2.75 cm^2 V^{-1} s^{-1} [36b]

(6)

Hexathienoacene   (HTA)
0.06 cm^2 V^{-1} s^{-1} [35j]

(7)

f-B5TB   0.5 cm^2 V^{-1} s^{-1} [35k]

(8)

TIPS

TIPS

(9)

BTQBT
0.2 cm^2 V^{-1} s^{-1} [40a]

(10)

DATT   3.0 cm^2 V^{-1} s^{-1} [37 (b)]

(11)

DNTT
R=C$_n$H$_{2n+1}$ 2.9 cm^2 V^{-1} s^{-1} [37 (a)]

(12)

DT-TTF
1.4 cm^2 V^{-1} s^{-1} [40 (b)]

(13)

Sii-Pr

Sii-Pr

P5-TIPSA 0.17 cm^2 V^{-1} s^{-1} [40c]

(14)

C$_{10}$H$_{21}$ C$_{10}$H$_{21}$

Dec-(TPhT)2-Dec 0.4 cm^{2}V^{-1}s^{-1} [40 (d)]

(15)

Rubene 40 cm^2 V^{-1} s^{-1} [35f]

(16)

R

R

R=Octylphenyl
OPIND
0.012 cm^2 V^{-1} s^{-1} [38a]

(17)

C$_8$H$_{17}$

C$_8$H$_{17}$

3POIND
0.2 cm^2 V^{-1} s^{-1} [38b]

(18)

H

H

DNPP
0.014 cm^2 V^{-1}s^{-1} [39]

(19)

C$_6$H$_{13}$ C$_6$H$_{13}$

DH-FlTTFl   0.1 cm^2 V^{-1} s^{-1} [40 (c)]

(20)

C$_6$H$_{13}$

C$_6$H$_{13}$

DH-PPTPP   0.02 cm^2 V^{-1} s^{-1} [40 (f)]

Figure 1. 7 Chemical structures of p-type small molecules used in transistors
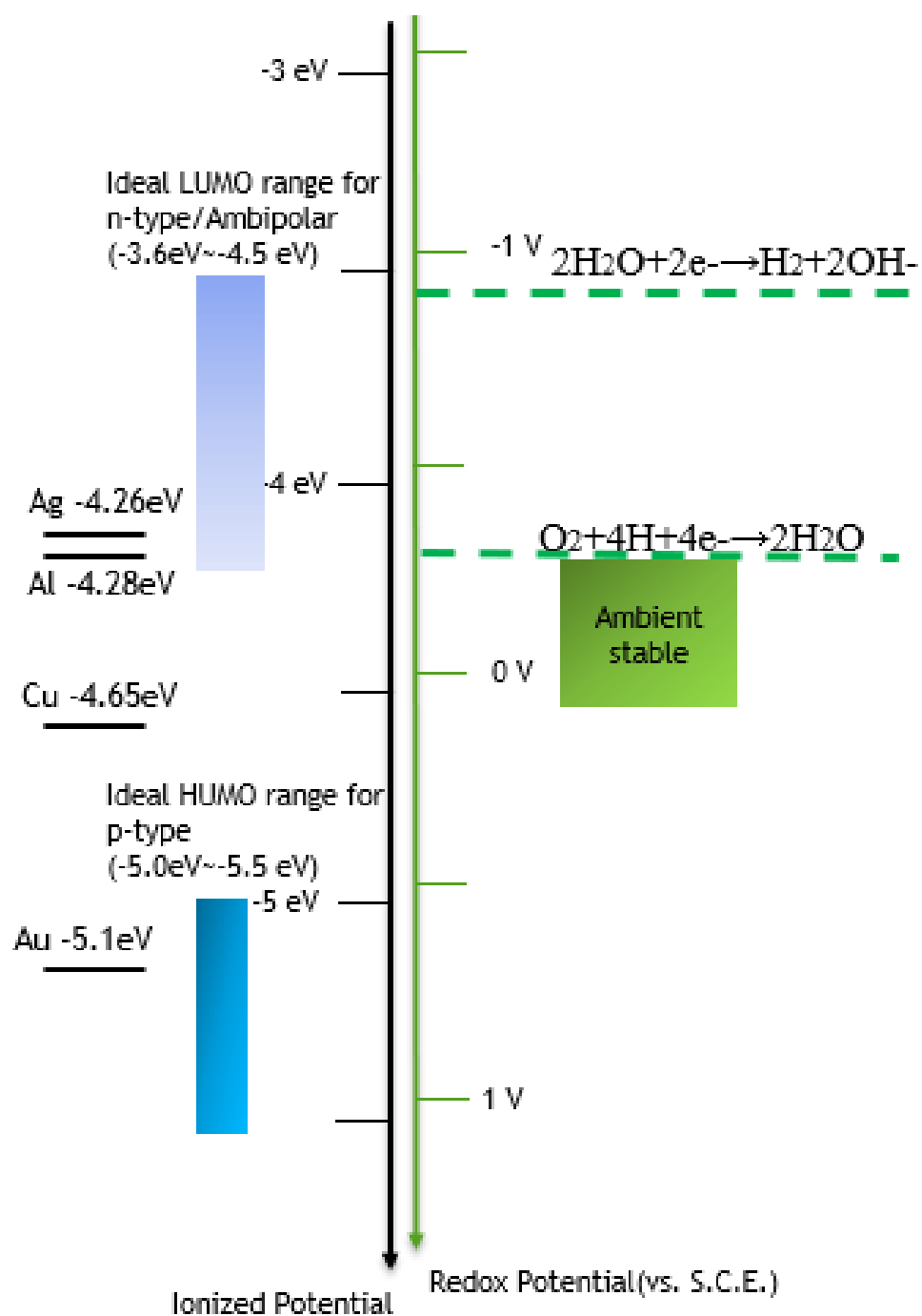
Figure 1. 8 Appropriate frontier molecular energy levels of organic semiconductors for OFETs [41]

From the perspective of molecular design, organic semiconductors are required to satisfy carrier injection and characteristics, so as to achieve the best performance in transistors. i) Proper molecular energy level **(Figure 1. 9):** for p-type semiconductors, HOMO level should be in the range of -5.0 eV to -5.5 eV for hole injection matching with Au electrode. [41] While the LUMO level of n-type semiconductors is generally lower than -4.0 eV to reduce the electron injection barrier height (ϕe) which is the difference between the LUMO energy of the semiconductor and the Fermi energy (E_F), which is also helpful for the air stability. [42] **Figure 1. 8** exhibits appropriate frontier molecular energy level for p-type or n-type semiconductors for organic field-effect transistors. ii) In order to migrate charge efficiently between the molecules, organic semiconductors should provide sufficient conjugated molecular overlap. [43,44] (iii) The extended π-conjugation framework and enhanced planarity of molecular backbone as a necessary condition ensure high charge carrier mobility. [45] (iv) Good film crystallinity that shows smaller π-π stacking distance and well-connected morphology with fewer grain boundaries will assist in boosting the electron coupling and improving charge transport. [46] (v) Introduction of soluble side chain to molecular backbone guarantee its solubility. [47]

1.2. Organic semiconductors containing lactam moiety

Lactam is a strong electron withdrawing group bearing carbonyl and amide moieties that can stabilize LUMO level to facilitate charge injection, which stimulated the interest of scientists along with widespread use in optoelectronic semiconductors. Acceptor with lactam group connected with donating unit can construct π-stacking structure owing to the strong intermolecular donor-acceptor interaction, leading high performance in transistors. Not only that, organic semiconductors containing lactam group have more advantages in extending π-conjugation, improving the co-planarity of molecule structure. In addition, The unsubstituted compound containing lactam unit is insoluble in common organic solvents, which is caused by strong intermolecular hydrogen bonds (between N-H and O) and π-π stacking interaction, so the most effective way to improve solubility is to introduce a soluble substituent at N atom of amide position. So far, increasing research about organic semiconductor containing lactam unit has been widely carried out in the world.
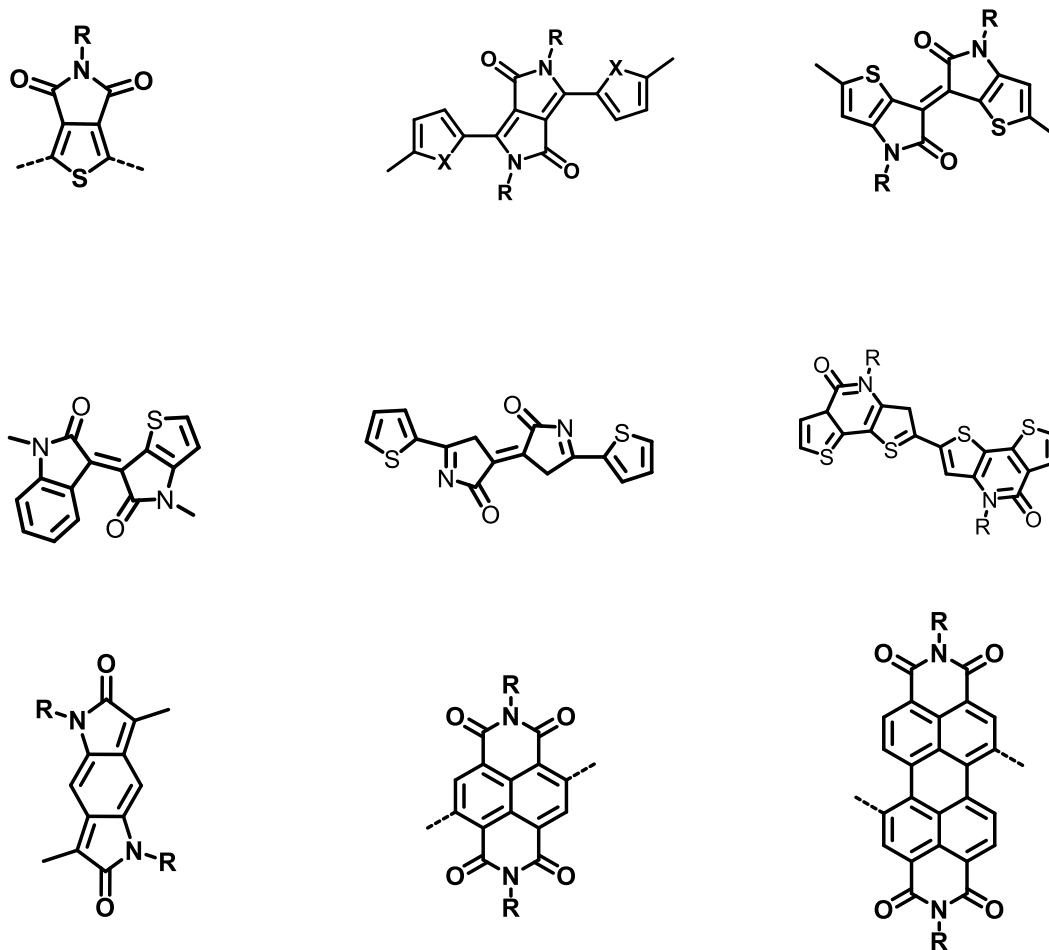
Figure 1. 9 Chemical structures of accepting building block with lactam groups.
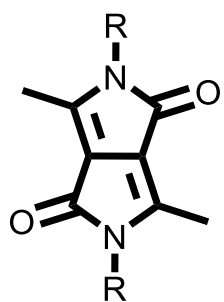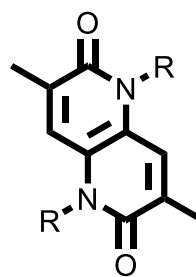
Diketopyrrolopyrroles   1,5−Naphthyridine−2,6−dione

Figure 1. 10 Chemical structures of Diketopyrrolopyrroles (DPP) and 1,5-Naphthyridine-2,6-dione (NTD)

1.2.1. Diketopyrrolopyrroles and their derivatives

Over the decades, diketopyrrolopyrrole (DPP) as a much-utilized and favorable accepting building block has attracted many research interests with a broad prospect in the π-conjugated system because of its excellent thermal stability, mechanical stability and air stability. On the one hand, strong intermolecular hydrogen bonds between adjacent molecules can contribute to realizing the planarity in DPP, further leading to the enhancement of π‑π stacking, which is beneficial to the ordering assembly of molecules and the migration of charges. On the other hand, there are multiple reaction sites on the molecular skeleton of DPP core using as a fused aromatic semiconducting moiety. [48] Not only can nucleophilic aromatic substitution reaction or electrophilic aromatic substitution be realized in an aromatic ring, but the presence of bis-lactam unit with a strong electron-deficient property make the synthesized DPP-based semiconductors have lower LUMO levels to realize the air stability. Also, solubility can also be improved by introducing alkyl chains into DPP cores to facilitate easy processing during the preparation of optoelectronic devices.

Importantly for use in OFET as an electron-deficient building block, the DPP motif is able to not only play an important role in tight π–π stacking but also enhance the charge delocalization of corresponding compounds owing to its high co-planarity and quinoidal structure, which is highly beneficial to charge-carrier transport through intermolecular charge hopping. [49,50] Therefore, DPP and its derivatives are widely used in organic light emitting dielectrode, [51] solar cells [52] and field effect transistors. [49]

Compared with small molecules, polymers have some limitations such as non-uniform molecular-weight distribution, time-consuming, the difference in molecular weight batch and the purity problem of polymer, resulted in the decrease of mobility. In addition, due to well-defined architecture, small molecules can easily self-assemble into the ordered structures and can be confirmed by crystal structure analysis. [53] Therefore, small molecules based on DPP unit have attracted extensive attention in recent years.

It is well known that the introduction of a fluorine substituent effectively reduces the energy level and also exerts considerable influence on the charge transport and molecular

orientation in solid state. [54] Y. Suna et al. introduced fluorine substituents into DPP core for the first time. Although the thin film transistor of this molecule shows ambipolar behavior, its mobility ($\mu_e = 10^{-4}$ cm^2 V^{-1} s^{-1}, $\mu_h = 10^{-5}$ cm^2 V^{-1} s^{-1}) is relatively low. [55] In 2014, Li Hongxiang and co-workers incorporated perfluorohexyl chain with stronger electron withdrawing ability into DPP core. Perfluorohexyl containing small molecule with lower HOMO and LUMO levels exhibited ambipolar characteristics. The hole mobility was 0.012 cm^2 V^{-1} s^{-1} and electrons of 0.011 cm^2 V^{-1} s^{-1}was appeared. [54]

1.2.2. Introduction of 1,5-Naphthyridine-2,6-dione (NTD)

The novel 1,5-naphthyridine-2,6-dione (NTD) acceptor was first reported by Yoon et al., which exhibits remarkably higher absorption coefficients, deeper highest occupied molecular orbital energy levels, and much more planar backbone structure than diketopyrrolopyrrole (DPP) induced by strong and favorable S-O interactions. [56]

As can be seen from the structure of NTD shown above, it includes a high electron affinity driven by electron withdrawing nature of the lactam units, possessing six-membered ring different from DPP. Not only that, NTD exhibits higher coplanarity of the conjugated structure owing to the intramolecular S⋯O interactions, which helps it have a good charge transport property. Also, it is a great soluble material through the introduction of various solubilizing side groups at lactam position. And it has a high absorption coefficiency, which makes it possible that NTD can show superior performance in the solar cell [56,57] and transistor. [58] Undoubtedly, the research on NTD accepting unit is necessary to continue to pursue and explore.

1.3. Research Objective

The aim of this research is to investigate the relationship in detail between the structure of small molecules, their electronic structure, optical and electrical properties, and processing in the application, which has aroused people's attention gradually in a field of material science and engineering. In particular, I was interested in the interplay of structure and property relationships, which is a significant issue for material design at a first level. It is highly significant to explore the correlation among structures and properties because supramolecular structures usually have a decisive impact on self-assembled properties, which are critical factors in performance of optoelectronic applications.

Over the decades, planar bis-lactam-based materials, such as diketopyrrolopyrrole (DPP) has attracted significant attention due to their high electron affinity driven by strong electron withdrawing characteristics of the lactam units, strong fluorescence characteristics, wide light absorption range, favorable quasi-planar backbone structures, as well as the facile control over the molecular orbitals (MOs), which cooperatively provide outstanding charge carrier transport efficiencies in organic photovoltaics (OPVs) and organic field-effect transistors (OFETs). [59] However, there is a natural tendency to develop a novel accepting unit to substitute DPP unit owing to the limitations of planarity of DPP unit.

Recently, we reported a new bis-lactam-based compound, naphthyridinedione (NTD), as a promising electron deficient building block, and developed NTD-based semiconducting donor polymers with high PCE (> 9%), much higher than corresponding polymer using DPP (3.26%) due to their outstanding absorption coefficient and dense $\pi-\pi$ stacking due to their outstanding absorption coefficient and dense $\pi-\pi$ stacking. [56,57] Meanwhile, NTDT showed outstanding p-type characteristics as a deposited OFET device with remarkable hole mobility of 1.29 cm^2 V^{-1} s^{-1} due to its specific crystal structure, 2D electronic coupling, etc. [58] But a systematic study of the structure-property relationship about NTD-based small molecules has not yet been reported.

Herein, we present a systematic study of the structure-property relationship about π-conjugated molecules based on NTDT substituted with hexyl side chains in different positions for use in organic field effect transistor in different processing. In order to explore

the effect of these NTDT series molecules on intermolecular interaction and molecular packing structure accurately, we introduce alkyl chain as substituent group instead of electron donating group or electron withdrawing group since the alkyl chain has minimal impact on the electronic conjugated structure of the backbone. Although changing the position of side chain has little influence on the optical absorption and emission in solution, it changes the optical properties, intermolecular interaction and molecular packing in the solid state, which is significant in the charge carrier transport and OFET performance significantly since It has been widespread reported that the charge transport properties and electronic characteristics depend on molecular structure and molecular packing. As a result, π–π stacking and further the carrier mobilities in the application can be controlled or tuned by alkyl chain engineering through precise chemical modification.

For basic studies on NTDT series molecules, intermolecular interaction and molecular structure stacking are expected to change in solid state by controlling planarization of molecules which caused by S···O secondary interaction, which can further cause the properties and performance of device change. And I also expected that NTD series named Octyl_NTDT_αhexyl, Octyl_NTDT_βhexyl, Octyl_NTDT_γhexyl with good solubility can exhibit saturation characteristics as p-type transistors using solution process technology.

1.4. Bibliography

[1] G.Gelinck, P.Heremans, K. Nomoto and T .D . Anthopoulos, *Adv. Mater.*, **2010**, 22, 3778–3798.

[2] T. Yokota, Y. Inoue, Y. Terakawa , J. Reeder , M. Kaltenbrunner , T. Ware , K. Yang , K. Mabuchi , T. Murakawa , M. Sekino , W. Voit , T. Sekitani and T. Someya, *Proc. Natl. Acad. Sci. U. S. A.*, **2015**, 112, 14533 -14538

[3] Lipomi D J, Vosgueritchian M, Tee B C-K, Hellstrom S L, Lee J A, Fox C H and Bao Z, Skin-like pressure and strain sensors based on transparent elastic films of carbon nanotubes *Nat. Nanotechnol.,* **2011**, 6, 788–92.

[4] K. J. Baeg, Y. Y. Noh, J. Ghim , S. J. Kang , H. Lee and D. Y. Kim , *Adv. Mater.*, **2006**, 18 , 3179 -3183.

[5] A. N. Sokolov, B. C.-K. Tee, C. J. Bettinger , J. B.-H. Tok and Z. Bao , *Acc. Chem. Res.*, **2012**, 45, 361 -371.

[6] J. F. Chang, B. Q. Sun, D. W. Breiby, M. M. Nielsen, T. I. Solling, M. Giles,I. McCulloch, H. Sirringhaus, *Chem. Mater.* **2004,** 16, 4772

[7] A. Tsumura, H. Koezuka, T. Ando, *Appl. Phys. Lett.*, **1986**, 49, 1210.

[8] Supriya Karmakar, Faquir C. Jain, *Silicon.,* **2016**, 8,369–379

[9] G. H.Gelinck, H. E. A Huitema, E. van Veenendaal, E. Cantatore, L. Schrijnemakers, J. B. P. H. van der Putten, T. C. T. Geuns, M. Beenhakkers, J. B. Giesbers, B-H. Huisman, E.J. Meijer, E. M. Benito, F. J. Touwslager, A. W. Marsman, B.J.E. van Rens, D. M. de Leeuw, *Nature Materials.*, **2004**. 3.106.

[10] Jurchescu, O. D., Popinciuc, M., van Wees, B. J., Palstra, T. T. M., *Adv. Mater.*, **2007**, 19, 688.

[11] Li, H., Tee, B. C. K., Cha, J. J., Cui, Y., Chung, J. W., Lee, S. Y., Bao, Z., J. Am. Chem. Soc. **2012**, 134, 2760.

[12] Christopher R. Newman, C. Daniel Frisbie, Demetrio A. da Silva Filho, Jean-Luc Bre´das, Paul C. Ewbank, *Chem. Mater.* **2004***,* 16, 23.

[13] Chong-an Di, Yunqi Liu, Gui Yu and Daoben Zhu, *Acc. Chem. Res.,* **2009**, 42, 10, 1573-1583.

[14] Y. Shirota, H. Kageyama, *Chem. Rev.*, **2007**, 107, 953.

[15] C. Wang, H. Dong, L. Jiang, W. Hu, *Chem. Soc. Rev.*, **2018**, 47, 422-500.

[16] C. Wang, H. Dong, W. Hu, Y. Liu, D. Zhu, *Chem. Rev.*, **2012**, 112, 2208-2267.

[17] C. Lu, Z. Ji, G. Xu, N. Lu, L. Li, M. Liu, *Org. Electron.,* **2017**, 49, 206-211.

[18] C.-A. Di, Y. Liu, G. Yu, D. Zhu, *Acc. Chem. Res.*, **2009**, 42, 1573-1583.

[19] Cheng liang Wang, Huanli Dong, Wenping Hu, *Chem. Rev.*, **2012**, 112, 4, 2208-2267.

[20] Marta Mas-Torrent, Concepcio Rovira, *Chem. Rev.*,**2011**, 11, 4833-4856.

[21] Yaochuan Mei, *Nanoelectronics*, **2019**, 115-129.

[22] AntonioFacchetti, *Materialstoday*, **2007**,10, 3, 28-37.

[23] (a) Jana Zaumseil, Henning Sirringhaus, *Chem. Rev.,* **2007**, 107, 4, 1296-1323. (b) Hamid Reza Barzegar, Christian Larsen, Nicolas Boulanger, Alex Zettl, Ludvig Edman, and Thomas Wågberg, *Nano Letters.*, **2018**, 2, 18, 2, 1442-1447. (c) Yu Liu, Feifei Wang, Junhui Chen, Xianghua Wang, Hongbo Lu, Longzhen Qiu, and Guobing Zhang, *Macromolecules*, **2018**, 51, 2, 370-378.

[24] Alessandra Operamolla and Gianluca M.Farinola, *Eur. J. Org. Chem.*, **2011**, 423-450.

[25] Yasuhiko Shirota, Hiroshi Kageyama, *Chem. Rev.*, **2007**, 107, 4, 953-1010.

[26] Zachary A. Lamport, Hamna F. Haneef, Sajant Anand, Matthew Waldrip, and Oana D. Jurchescu, *Journal of Applied Physics.,* **2018**, 124, 7, 110.

[27] X. Tao, V. Koncar, *Smart Textiles and their Applications*, **2016**, 569-598.

[28] Bisri S Z, Takenobu T, Takahashi T, et al., *Appl Phys Lett*, **2010**, 96, 18, 90-98.

[29] Ahn H, Ohno A, Hanna J., *J Appl Phys*. **2007**, 102, 7, 937-945.

[30] Hong J P, Park A Y, Lee S, *Appl Phys Lett*, **2008**, 92, 14, 131-137.

[31] Dong HL, Jiang L, Hu WP, *Phys Chem Chem Phys*, **2012**, 14, 41, 14165-14180.

[32] Janos Veres, Simon Ogier, Giles Lloyd, Dago de Leeuw, *Chemistry of Materials*, **2004**, 16, 23, 4543-4555.

[33] (a) Takefumi Odajima, Minoru Ashizawa, Yuichi Konosu, Hidetoshi Matsumotoa, Takehiko Mori, *J. Mater. Chem. C*, **2014**, 2, 10455 –10467. (b) Shi Ya-Rui, Wei Hui-Ling, Shi Ya-Ting and Liu Yu-Fang, *CrystEngComm*, **2017**,19, 6008.

[34] (a) Jie Yang, Zhiyuan Zhao, Shuai Wang, Yunlong Guo, Yunqi Liu, J. *Chem.*, **2008**, 4, 12, 2748-2785. (b) Alessandra Operamolla, Gianluca M. Farinola, *Eur. J. Org. Chem.*, **2011**, 423–450.

[35] (a) Klauk H, Halik M, Zschieschang U, Eder F, Schmid G., and Dehm C. *Appl. Phys. Lett.,* **2003**, 82, 4175. (b) OD Jurchescu, J. B., TTM Palstra., *Appl. Phys. Lett .***2004**, 84, 16, 3061-3063. (c) Anthony J E, Brooks J S, Eaton D L, et al., *J. Am. Chem. Soc.* **2001**, 123, 38, 9482-9483. (d) Ze-Fan Yao, Jie-Yu Wang, Jian Pei, *Crystal Growth & Design*, **2018**, 18, 1, 7-15. (e) Okamoto, H, Kawasaki. N, Kaji. Y, Kubozono, Y, Fujiwara. A, Yamaji, M, *J. Am. Chem. Soc,* **2008**, 130, 32, 10470-10471. (f) Wang, C. L, Liu, Y. L, Ji, Z. Y, Wang, E. J, Li, R. J, Jiang, H, Tang, Q. X. Li, H. X, Hu, W. P, Cruciforms, *Chem Mater*, **2009**, 21,13, 2840-2845. (g) Takimiya. K, Kunugi, Y. Konda, Y. Ebata, H. Toyoshima, Y. Otsubo, *J. Am. Chem. Soc.* **2006**, 128, 9, 3044-3050. (h) Tang M L, Okamoto T, and Bao Z. *J. Am. Chem. Soc.* **2006**, 128, 16002. (i) Xiao. K, Liu. Y. Q, Qi. T. Zhang, W. Wang, F. Gao, J. H, Qiu, W. P, Zhu, D. B, *J. Am. Chem. Soc*. **2005**, 127, 38, 13281-13286. (j) Liu. Y, Sun. X. N, Liu. Y. Q, Du. C. Y, Lu. K, Ye. S.　H, Yu. G, *Chem. Asian.* **2010**, 5, 7, 1550-1554. (k) Yamada K, Okamoto T, Kudoh K, et al, *Appl. Phys. Lett.* **2007**, 90, 7, 72-102.

[36] (a) Izawa. T, Miyazaki. E, Takimiya. K, *Adv. Mater.,* **2008**, 20, 18, 3388-3392. (b) Ebata. H, Izawa. T, Miyazaki. E, et al., *J. Am. Chem. Soc.,* **2007**, 129, 51, 15732-15733.

[37] (a) Yamamoto. T, Takimiya. K, *J. Am. Chem. Soc.*, **2007**, 129, 8, 2224-2225. (b) Takimiya. K, Kunugi. Y, Otsubo. T, *Chem. Lett.*, **2007**, 36, 578.

[38] (a)Wu Y, Li Y, Gardner S, Ong BS, *J Am Chem Soc.* **2005,** 127, 2, 614-618. (b)Pierre-Luc, T, Boudreault, Salem Wakim, Nicolas Blouin, Michel Simard, Christian Tessier, Ye Tao, Mario Leclerc, *J. Am. Chem. Soc.*, **2007**, 129, 29.

[39] Li Qiu, Chunmeng Yu, Na Zhao, Weichao Chen, Yunlong Guo, Xiaobo Wan, *Chem. Commun.,* **2012**, 48, 12225-12227.

[40] (a) Masaki Takada, Harald Graaf1, Yoshiro Yamashita, Hirokazu Tada1, *Jpn. J. Appl. Phys.,* **2002,** 41, 4–6. (b) Marta Mas-Torrent, Murat Durkut, Peter Hadley, Xavi Ribas, Concepció Rovira, *J. Am. Chem. Soc.* **2004**, 126, 4, 984-985. (c) J.E. Anthony, et al., *J. Am. Chem. Soc.,* **2001**, 123, 9482-9483. (d) S.A. Ponomarenko, et al., *Chem. Mater.*, **2006**, 18, 579-586. (e) H. Meng, et al. *J. Am. Chem. Soc.*, **2001**, 123, 37, 9214-9215. (f) Melissa Mushrush, Antonio Facchetti, Michael Lefenfeld, Howard E. Katz, Tobin J. Marks, *J. Am. Chem. Soc*. **2003**, 125, 31, 9414-9423.

[41] Alessandra Operamolla, Gianluca M. Farinola, *Eur. J. Org. Chem*., **2011**, 423–450.

[42] Jesse T. E. Quinn, Jiaxin Zhu, Xu Li, Jinliang Wang, Yuning Li, *J. Mater. Chem. C*,

2017, 5, 8654-8681.

[43] Antonio Facchetti, *Materialstoday,* **2007**, 10, 3, 28-37.

[44] D. Fichou, G. Horowitz, *Encyclopedia of Materials: Science and Technology,* **2001**, 5748-5757.

[45] Huanli Dong, Xiaolong Fu, Jie Liu, Zongrui Wang, Wenping Hu, *Adv.Mater.*, 2013, 25, 6158–618.

[46] S. Xu, N. Ai, J. Zheng, N. Zhao, Z. Lan, L. Wen, X. Wang, J. Pei and X. Wan, *RSC Adv.*, 2015, 5, 8340–8344.

[47] J. E. Anthony, J. S. Brooks, D. L. Eaton and S. R. Parkin, *J. Am. Chem. Soc.*, **2001**, 123, 9482–9483.

[48] Qian Liu, Huabin Sun, Chula Blaikie, Chiara Caporale, Sergei Manzhos, Krishna Feron, Jennifer M. MacLeod, Massimiliano, Yong-Young Noh, Prashant Sonar, *New J. Chem.*, **2018,** 42, 12374-12385.

[49] L. Huo, J. Hou, H.-Y. Chen, S. Zhang, Y. Jiang, T. L. Chen and Y. Yang, *Macromolecules*, **2009**, 42, 6564–6571.

[50] Y. Li, P. Sonar, S. P. Singh, M. S. Soh, M. van Meurs and J. Tan, *J. Am. Chem. Soc.*, **2011**, 133, 2198–2204.

[51] Meirong Chen , Weifei Fu , Hongzheng Chen, *J. Mater. Chem. A*, **2013**, 1, 105-111.

[52] Derong Cao, Qilin Liu, Wenjing Zeng, Shaohu Han,Junbiao Peng, Shouping Liu, *Macromolecules*, **2006**, 39, 24, 8347-8355.

[53] Chenmin Yu , Chang He , Yang Yang , Zhengxu Cai , Hewei Luo , Wenqiang Li , Qian Peng , Guanxin Zhang , Zitong, *Chem. Asian J.*, **2014**, 9, 1570-1578.

[54] Yuanyuan Wang, Qiuliu Huang, Zhiqing Liu, Hongxiang Li, *RSC, Adv.*, **2014**, 4, 29509-29513.

[55] S. Liu, M. Shi, J.Huang, Z.Jin, X.Hu, J. Pan, H. Li, A. K.-Y.jen, H. Chen, *J. Mater.Chem. A.*, **2013**, 1, 2795.

[56] Won Sik Yoon, Dong Won Kim, Jun-Mo Park, Illhun Cho, Oh Kyu Kwon, Dong Ryeol Whang, Jin Hong Kim, Jung-Hwa Park, Soo Young Park, *Macromolecules,* **2016**, 49, 22, 8489–8497.

[57] Won Sik Yoon, Dong Won Kim, Min-Woo Choi, Jun-Mo Park, Soo Young Park, *Adv. Energy Mater.*, **2018**, 8, 1701467.

[58] Jin Hong Kim, Min-Woo Choi, Won Sik Yoon, Sangyoon Oh, Seung Hwa Hong, Soo Young Park, *ACS Applied Materials & Interfaces*, 2019, 11, 8301−8309.

[59] Ailing Tang, Chuanlang Zhan, Jiannian Yao, Erjun Zhou, *Adv. Mater.,* **2017**, 29, 1600013.

Chapter 2.　Study on Structure-Property Relationship of 1,5-naphthyridine-2,6-dione (NTD) cores with Tuning Alkyl Group

2.1. Introduction

In 1974 Farnum et al.found and synthesized diketopyrrolopyrrole (DPP) pigment for the first time, and then the DPP derivatives as lactam-containing organic semiconductor are getting attention owing to the electron-withdrawing properties, outstanding physiochemistry characteristics and planarity of DPP motif attributed to strong intermolecular hydrogen bond and large area π-conjugated overlaps with the deepening of its application. [1] Due to these advantages, the DPP derivatives are gradually becoming the core materials applied in OFET, and a lot of researches on DPP are in progress in the world.

However, the backbone of DPP-based derivatives is able to be tilted from coplanarity with torsional angle when it symmetrically substituted with various heteroaromatic moieties, which may be one of the important reasons which cause the difficulties in performance improvement. In these days, most of the mobility of DPP-small molecules is at $10^{-2}\,cm^2\,V^{-1}\,s^{-1}$ level and transistors were prepared through vacuum deposition or thermal annealing spin-coating. The poor solubility of DPP is also recognized as a serious limitation for processing of devices. Therefore, substitution of alkyl chain is often carried out on its amide nitrogen position to improve its solubility. And it has been widely reported that introduction of side chain with different alkyl spacer lengths and different types also have a significant influence on the electrical properties of small molecular derivatives have been reported in the literature. [2,3,4] So, the difficulties in improving the charge transport of DPP transistors mainly arise due to the presence of these defects.

In order to solve the problem, our lab designed a novel planar 1,5-Naphthyridine-2,6-dione (NTD) unit for the first time in the world. 3,7-di (thiophene-2-yl)-1,5-naphthyridine-2,6-dione (NTDT), an aromatic molecule with 10π electrons exhibits distinguishing features such as strong absorption coefficient, thermodynamic stability, mechanical

stability and so forth. [5] In addition, novel NTD accepting building block with two lactam structures shows a strong electron deficient property and it also displays strong fluorescence intensity due to the specific aromatic characteristics. [6] Intermolecular interaction about S···S and S···O, and the C–H···O═C intermolecular interactions could be occurred by the molecular conformation between the disubstituted thiophene donating unit and the central bis-lactam core, which resulted in the strong co-planarity in NTDT favorable for charge transport. [7] Through the analysis of single crystal structure, NTDT showed strong two-dimensional intermolecular interactions including face-to-edge interaction as well as face-to-face interaction, leading to flat and uniform morphology, which is beneficial to high charge carrier mobility in the thin-film transistor. [7] While DPPT only has 1D intermolecular interaction with face to face interaction.

Based on the above description and discussion, NTDT based polymers were synthesized by Yoon et al. and distinguished performance was discovered in Organic photovoltaics with high PCE (>9%) [8,9]. So, NTDT motif was expected to be very favorable for charge transport. However, considering some problems in polymers such as time-consuming for synthesis, the rigorous and tough condition and difficulties in molecular weight batch control, which even lead low charge carrier mobility in transistors, Kim et al. fabricated thin-film transistor with high mobility of 1.29 cm^2 V^{-1} s^{-1} using NTDT small molecule since small molecules have more advantages of well-defined structures, high purities, a high degree of molecular ordering, precise molecular weights compared with polymers. [7] And NTDT molecule can provide a favorable 2D-like layer-by-layer growth mode by the analysis of morphology, which had a positive effect on transistor performance. While DPPT transistor only had 2.7×10^{-2} cm^2 V^{-1} s^{-1} with one-dimensional electron coupling. Therefore, systematic study and research about OFET based on NTDT derivatives are indispensable and necessary to do.

Herein, I studied the structure-property relationship about NTDT derivatives because few studies have been made on NTD building block. First, the basic chemical properties of NTD accepting unit have been studied. Then, I paid attention to the design strategies of organic semiconductors for transistors. When we design the molecular structure, modification of conjugated backbone and the selection of flexible side chain must be considered since the construction of conjugated backbone that allows controlling the

energy levels of the HOMO and LUMO frontier orbitals so as to realize the tunability of band gap and the electronic properties of the materials. [10] Also, attaching alkyl chains endowed with solubility can not only improve solution-processability of semiconducting molecules but also have a considerable impact on controlling self-assembly properties[11]. Moreover, the strategy of introducing solubilizing groups as auxiliary groups at N-position is also proved to be helpful for the molecular arrangement to enhance π−π orbital overlaps. [12] To date, there are numerous studies on molecular side chain engineering. Veronique S. Gevaerts et.al reported that the position of the side chains also can control the crystallization and the morphology. And changing the position of side chain is developed as a means of influencing optical and electronic properties of these molecules in thin semicrystalline films and therefore the performance of terminal device. [13] Gabriela Wiosna-Salyga and co-workers developed a series of compounds comprising a diketopyrrolopyrrole central accepting unit symmetrically disubstituted with thiophene units. It is found that the position of the alkyl substituent in the bithiophene could affect geometry and the potential of the first oxidation process since they had different dihedral angle between the two adjacent thiophene rings. [14]

So, in this work, on the basis of NTDT backbone with good transistor characteristic, I designed to incorporate alkyl chain as solubilizing groups without π electrons to investigate the effects of the self-assembly properties of the small molecules and molecular packing by changing the position of the solubilizing alkyl group on the thiophene unit for use in transistors. Design principles mainly followed by two parts: on the one hand, alkyl chains as solubilizing groups are beneficial for the solution processing of semiconductor. On the other hand, changing the position of alkyl chains with less electronic effect on conjugated backbone has an impact on the self-assembly properties and crystalinity.

A series target material of NTDT derivatives were successfully synthesized and optical and electrochemical properties were characterized. Geometry difference of target molecules was discovered by changing the position of N-substituent as shown in DFT calculation. Through those phenomena mentioned above, intermolecular interaction and crystallinity are expected to be changed in solid state by controlling planarization of molecules caused by S⋯O secondary interaction, which resulted in differences of optoelectronic properties and transistor performance. Typical p-type transistors

characteristics of NTDT series named Octyl_NTDT_αhexyl, Octyl_NTDT_βhexyl, and Octyl_NTDT_γhexyl with good solubility are expected to be achieved using vapor-deposited technology and solution processed technology.
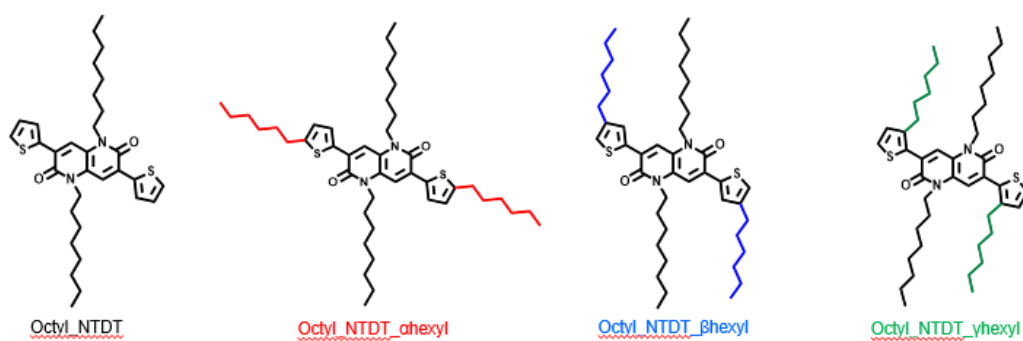
Scheme 2. 1 First target molecules for basic studies on structure-property relationships

2.2. Experimental

2.2.1. Synthesis
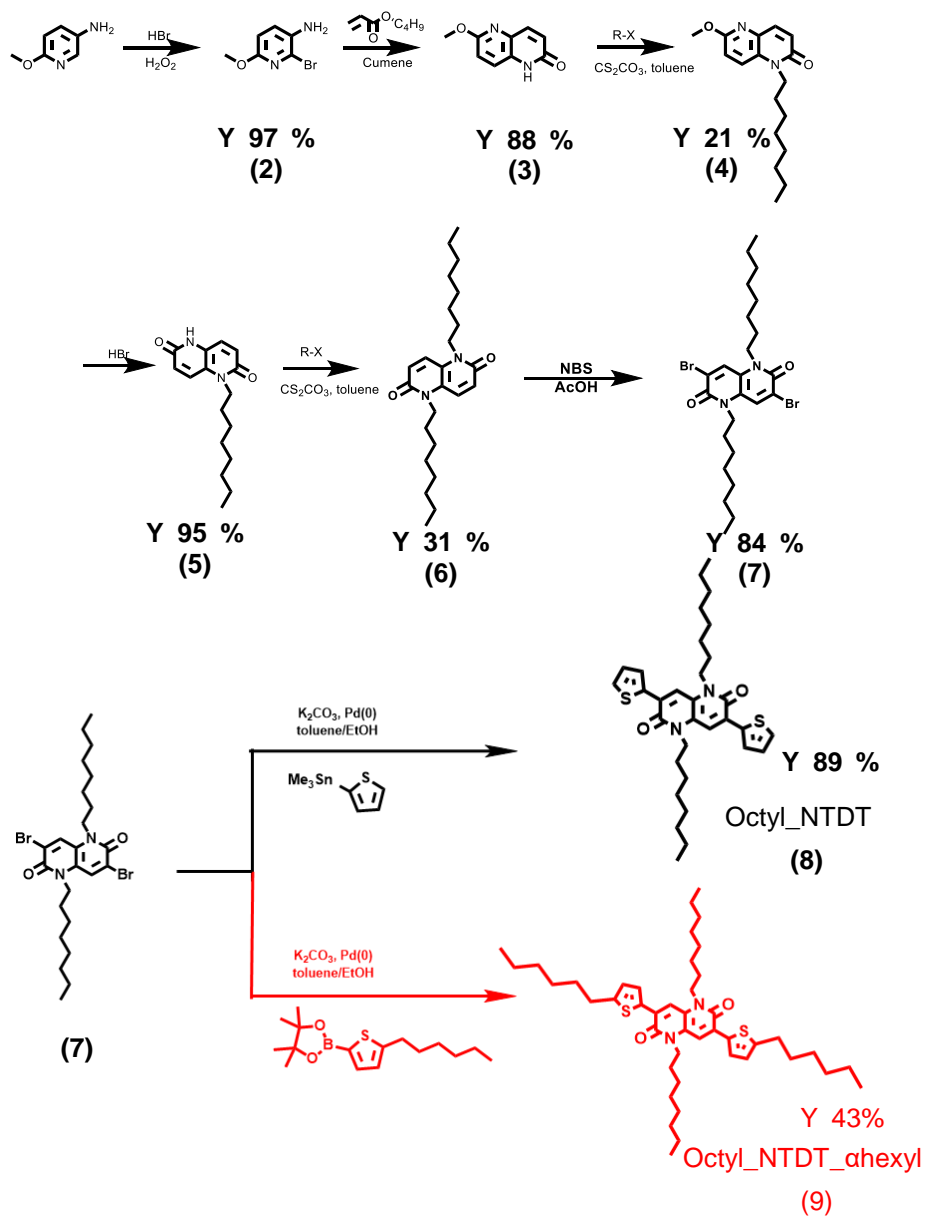
Scheme 2. 2 Synthetic route of Octyl_NTDT, Octyl_NTDT_αhexyl
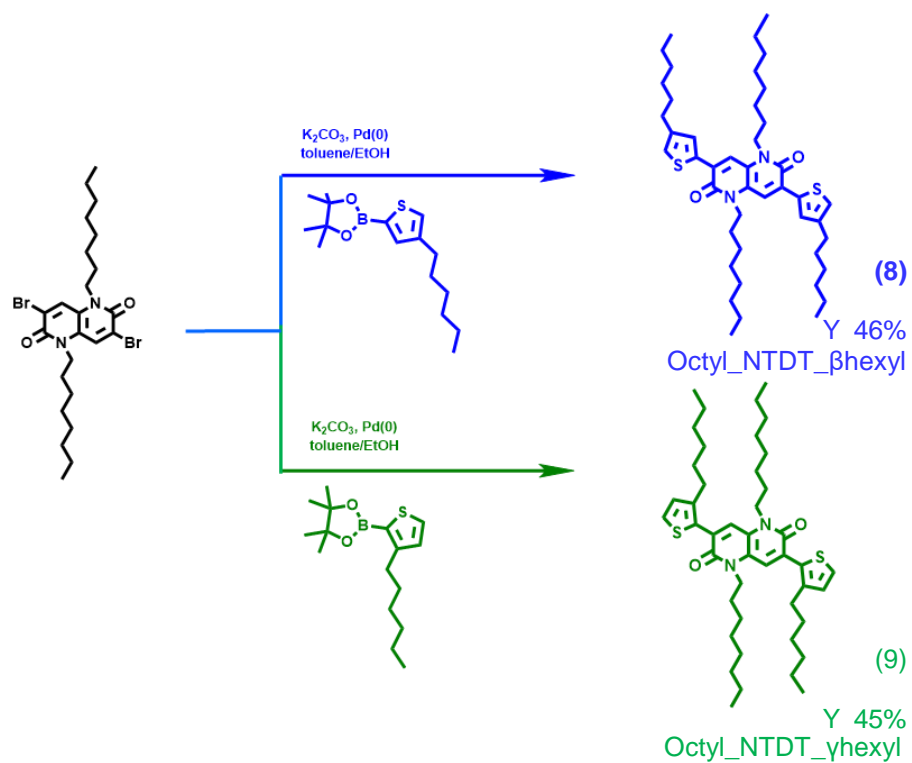
Scheme 2. 3 Synthetic route of Octyl_NTDT_βhexyl and Octyl_NTDT_ γhexyl.

All the reagents and solvents which involved in the experiment each process were bought from Sigma Aldrich, TCI Chemicals, Acros Organics, and Alfa Aesar.

Scheme 2. 2 showed a synthesis route of NTD-based small molecules. 6-bromo-5-amine-2-methoxypyridine (2) could be readily obtained by bromination reaction. Then,the aromatic ring was closed using and butyl acrylate as base and tri-tert-butylphosphine ligand/ palladium catalyst system through heck reaction to prepare compound (3). After the alkylation of compound of 1-octyl-1,5-naphthyridine-2,6-dione (4), O-demethylation was subsequently adopted to obtained (5) using hydrogen bromide. Attaching octyl on the other side through N-alkylation to obtain compound (6), which could react with N-Bromosuccinimide in ice bath to prepare precursor (7) coupling with bromine by bromination. The synthetic roots of this precursor (7) were obtained according to the literature. [8,9]

Synthesis of 1,5-dioctyl-3,7-dithiophen-2-yl-1,5-naphthyridine-2,6-dione (8, Octyl_NTDT).

Precursor (7) (2 g, 4.53 mmol), tributyl(thiophene-2-yl)stannane (2.5 g, 11.34 mmol) and Pd(PPh$_3$)$_4$ were added into a two-necked 500 mL round-bottom flask, then 40 mL DMF was put into the round-bottom flask. the solution was heated to 130°C and stirred with reflux tube under shading place overnight. After reaction finished, cooled the mixture with ice water and extracted with MC. The crude mixture was purified by column chromatography. The red solid product could be yielded according to the literature. [8] (3.47 g Yield: 83.56 %). 1H NMR (300 MHz, CDCl3, δ): δ 7.97 (s, 2H), 7.78 (d, J = 3.8 Hz, 2H), 7.54 (d, J = 5.3 Hz, 2H, 7.18 (t, J = 4.5 Hz, 2H), 4.43 (t, J = 8.0 Hz, 4H), 1.85 (m, 4H), 1.36-1.21 (m, 20H), 0.98 – 0.83 (m, 6H).

Synthesis of 3,7-bis(5-hexylthiophene-2-yl)-1,5-dioctyl-1,5-dihydro-1,5-napthyridine-2,6-dione (9, Octyl_NTDT_αhexyl)

Compound (9) was prepared by Suzuki coupling. the precursor (7) (500 mg, 0.91 mmol), 5-Hexyl-2-thiopheneboronic acid pinacol (811 mg, 2.75 mmol) and 25 mL toluene were added in a two-necked 100 mL round-bottom flask, then 695 mg of potassium carbonate mixed with 5 ml ethanol (EtOH) to form 1M solution was also put into the round-bottom flask. Then Pd(PPh$_3$)$_4$ using as catalyst were dissolved into the solution under the shading condition. The solution was stirred and refluxed at 80 °C overnight. When the reaction was completed, the temperature was cooled to room temperature. The mixture was extracted by dichloromethane, washed with brine and water, dried with MgSO$_4$. After evaporated, the as-prepared crude was purified by silica gel column chromatography using methylene dichloride and n-Hexane (MC:Hexane = 4:1) as eluent system. After that, recrystallization using methanol (MeOH) was carried out to separate the desired product at least three times. The red solid product was obtained after drying under vacuum. (283 mg, Yield: 43%)

1H NMR (300 MHz, CDCl3, δ): δ 7.87 (s, 2H), 7.61 (d, J = 3.7 Hz, 2H), 6.84 (d, J = 3.7 Hz, 2H), 4.39 (m, 4H), 2.87 (t, J = 7.6 Hz, 4H), 1.82 (m, 4H), 1.81 – 1.61 (m, 4H), 1.58 – 1.16 (m, 32H), 0.96 – 0.73 (m, 12H).

Synthesis of 3,7-bis(4-hexylthiophene-2-yl)-1,5-dioctyl-1,5-dihydro -1,5-naphthyridine-2,6-dione (10, Octyl_NTDT_βhexyl)

In a two-necked 100 mL round-bottom flask, the precursor (7) (1 g, 1.83 mmol), 2-(4-Hexyl-2-thienyl)-4,4,5,5-tetramethyl-1,3,2-dioxaborolane (1.62 g, 5.51 mmol) and Pd(PPh$_3$)$_4$ (0.21 g, 0.18 mmol) were dissolved into 40 mL toluene. 1.11 g of potassium carbonate dissolved into 8 mL ethanol (EtOH) and made into 1M solution, which was also put into the round-bottom flask. The mixture was stirred and refluxed at 80 °C overnight with light shielding. After reaction completed, cooled the mixture with ice water and extracted with MC, the crude was dried by vapor evaporation. Red solid could be obtained by silica gel column chromatography using methylene dichloride and n-Hexane (MC:Hexane = 3:1) as eluent system and recrystallization using methanol (MeOH). (607 mg, Yield: 46%). ^{1}H NMR (300 MHz, CDCl3, δ): δ 7.90 (s, 2H), 7.66 (s, 2H), 7.11 (s, 2H),

4.41 (m, 4H), 2.66 (t, J = 7.8 Hz, 4H), 1.83 (m, 4H), 1.67 (m, 4H), 1.32 (m, 16H), 0.99 –
0.79 (m, 6H).

Synthesis of 3,7-bis(3-hexylthiophene-2-yl)-1,5-dioctyl-1,5-dihydro -1,5-naphthyridine-2,6-dione (11, Octyl_NTDT_γhexyl)

Compound (11) was prepared by Suzuki coupling. the precursor (7) (500 mg, 0.91 mmol), 2-(3-Hexyl-2-thienyl)-4,4,5,5-tetramethyl-1,3,2-dioxaborolane (811 mg, 2.75 mmol) and Pd(PPh$_3$)$_4$ (0.11 g, 0.09 mmol) were added in a two-necked 100 mL round-bottom flask, 0.55 g of potassium carbonate dissolved into 4 mL ethanol (EtOH) and made into 1M solution, and 20 mL toluene were taken into the round-bottom flask. The mixture was stirred and refluxed at 80 °C overnight under shading place. When the reaction was completed, cooled the mixture with ice water,then extracted with methylene dichloride and . The extracts were combined and washed with water and then dried over anhydrous MgSO$_4$. Then the crude should be purified by silica gel column chromatography using methylene dichloride and n-Hexane (MC:Hexane = 5:1) as eluent system and then recrystallized using methanol. Finally, the red solid could be obtained after drying by vacuum oven. (297 mg, Yield: 45%). 1H NMR (300 MHz, CDCl3, δ): δ 7.66 (s, 2H), 7.44 (d, J = 5.2 Hz, 2H), 7.04 (d, J = 5.2 Hz, 2H), 4.31 (t, J = 8.0 Hz, 4H), 2.83 – 2.67 (m, 4H), 1.80 (q, J = 7.4 Hz, 4H), 1.68 (q, J = 7.7 Hz, 4H), 1.51 – 1.08 (m, 32H), 0.87 (td, J = 6.8, 5.5, 3.1 Hz, 12H).

2.2.2. Instruments and measurements

Chemical structures of synthesized molecules were identified with ^{1}H NMR (TMS is an internal standard) using Bruker, Avance-300 type. Density functional theory (DFT) using Gaussian09 at B3LYP/6-31G* level is a kind of calculating frontier molecular orbital energy level instrument which can get the information about energy level.

Optical characteristics of the compounds were investigated through UV-Vis spectra (SHIMADZU UV-1650PC). Reduction and oxidation processes of target molecular species were investigated utilizing cyclic voltammetry (CV, Princeton Applied Research, 273 A), in which we could get information of frontier molecular orbital energy level. Here, CV was employed to investigate HOMO levels of NTD derivatives both in solution state and solid state. I chose the electrolysis cell comprising a platinum working electrode composed of redoxinert material, a counter electrode using platinum wire, and an Ag^+/Ag pseudoreference electrode regarded as a reference electrode, respectively. The HOMO level of thin film was detected using 0.1 M of tetrabutylammonium hexafluorophosphate (TBAHFP) in acetonitrile (ACN) as supporting electrolytes, and the energy level in solution state was investigated utilizing 0.1 M of tetrabutylammonium tetrafluoroborate (TBATFB) in dichloromethane (DCM). The LUMO levels both in solution and solid state could be measured by the optical onset wavelength in UV/Vis spectroscopy and HOMO levels detected by CV.

The melting temperature of the molecules was determined by DSC (TA instruments, Q1000) under N_2 atmosphere. Studies on decomposition temperature of target molecules were carried out by thermal gravimetric analyzer (Discovery TGA) under N_2 atmosphere with a temperature range of 40~ 600 ℃, and the heating rate was 10 ℃/ min.

Degree of molecular stacking and crystallinity of compounds was analyzed by X-Ray Diffractometer XRD using D8-Advance (XRD, a1 system). Morphology of the thin film was investigated by optical microscopy (OM).

2.2.3. Fabrication and evaluation of OFETs

Vapor-Deposited Film and Device Fabrication:

Organic field effect transistors based NTDT derivatives named Octyl-NTDT-αhexyl, Oct-NTDT-βhexyl and Oct-NTDT-γhexyl were fabricated with bottom gate-top contact architecture by vacuum deposition on the ODTS self-assembled SiO_2/Si substrate. Before the preparation of thin films, SiO_2/Si substrates were cleaned with acetone, dichloromethane, isopropyl alcohol and tetrahydrofuran, respectively for 10 min with ultrasonication. Then substrates were dried overnight in vacuum oven and treated with UV-ozone after being dried by nitrogen. Subsequently, dried substrates were placed into an ODTS vapor chamber at 80 °C for 2.5 h to form ODTS monolayer in vacuum atmosphere. Through vacuum evaporation equipment, organic semiconductors (Octyl-NTDT-αhexyl, Octyl-NTDT-βhexyl and Octyl-NTDT-γhexyl) were sublimated and deposited on OTS-modified substrates at different annealing temperature with the rate of 0.1 Å/s under a pressure of $3×10^{-6}$ Torr (thickness of the films was controlled at 50 nm). Deposition of 50 nm thick gold electrodes was completed through a metal mask.

The mobility can be measured in the saturated region:

$$\mu_{sat.(VG)} = \cdot \frac{\partial IDS,sat}{\partial VG} \cdot \frac{L}{WCi} \frac{1}{VG - VT}$$

where C_i is the capacitance per unit area of the insulating layer, W is the channel width, L is the channel length, and μ is the field effect charge mobility. [10]

Solution-Processed Film and Device Fabrication:

All the target materials were dissolved into chloroform to prepare 10 mg/mL solution and stirred overnight. As-prepared solution was then filted by syringe filter and spin-coated onto the cleaned substrates at 5000 rpm to form uniform film. In order to anneal in various temperature, the spin-coated film was annealed at 70 °C, 110 °C for 10 min, respectively. Finally, 50 thick of gold electrodes were thermally deposited through a metal mask.

The mobility can be measured in the saturated region:

$$\mu_{sat.(VG)} = \cdot \frac{\partial IDS,sat}{\partial VG} \cdot \frac{L}{WCi} \frac{1}{VG - VT}$$

where C_i is the capacitance per unit area of the insulating layer, W is the channel width, L is the channel length, and μ is the field effect charge mobility. [10]

2.2. Results and Discussion

2.3.1 Theoretical molecular orbital calculation used density functional theory (DFT)

The electronic distribution and frontier orbital energy levels of NTD derivatives have been studied using Hartree-Fock/Density Functional Theory method with B3LYP with 6-31G (d,p) basis set. According to the density functional theory (DFT), HOMO and LUMO are mainly delocalized on the NTDT backbone since the alkyl chain with less electron effect has minimal impact on the electronic conjugated structure of the backbone. So there was no significant difference in energy levels at NTD series in isolated state. Calculated frontier molecular orbital (FMO) energy levels of target molecules can be seen from **Figure 2. 1.**

It is noteworthy that dihedral angle between NTD core and thiophene ring at Octyl_NTDT_αhexyl, Octyl_NTDT_βhexyl, and Octyl_NTDT_γhexyl are 1.38°, 1.47°, 2.51°, 30.35° respectively. Dihedral angle is dependent on the position of the alkyl solubilizing groups in the thiophene ring, being increased by changing the alkyl substituent position from α-position to γ-position. Octyl_NTDT_γhexyl is more distorted due to the steric hindrance compared with oct_NTDT. However, there is little change in dihedral angle at Octyl_NTDT_αhexyl, Octyl_NTDT_βhexyl compared with oct_NTDT. These phenomena also can be seen from side view in **Figure 2. 2.** So, Octyl_NTDT_αhexyl and Octyl_NTDT_βhexyl have favorable planar structure, leading effective extension of π-conjugation and intermolecular π–π interactions, which is beneficial for the mobility hopping in transistors.
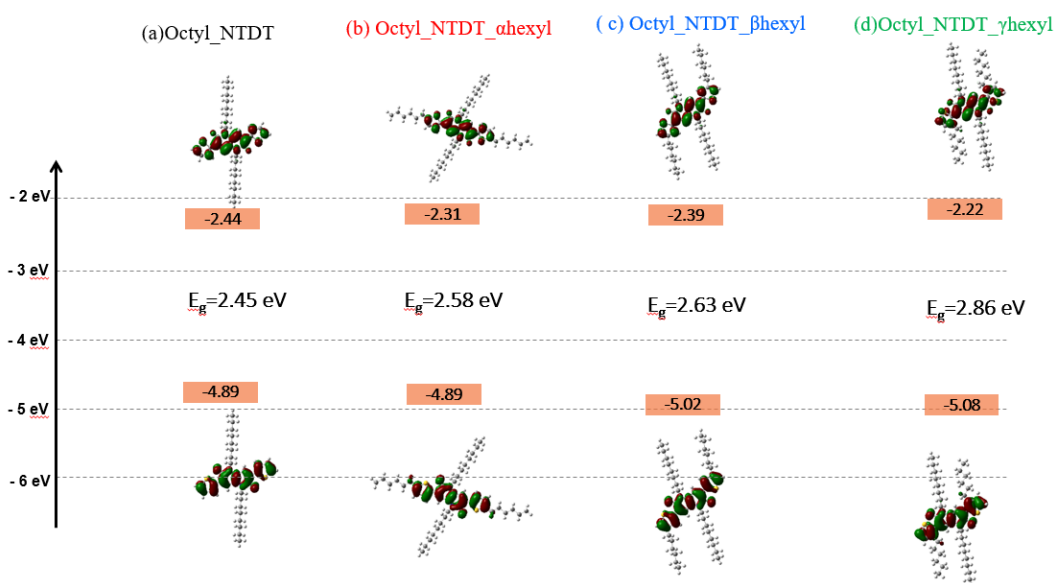
Figure 2. 1 Calculated frontier molecular orbital (FMO) energy levels and electron density maps of (a) Octyl_NTDT, (b) Octyl_NTDT_αhexyl, (c) Octyl_NTDT_βhexyl, and (d) Octyl_NTDT_γhexyl . Calculation method was DFT and basis set was B3LYP/6-31G*.
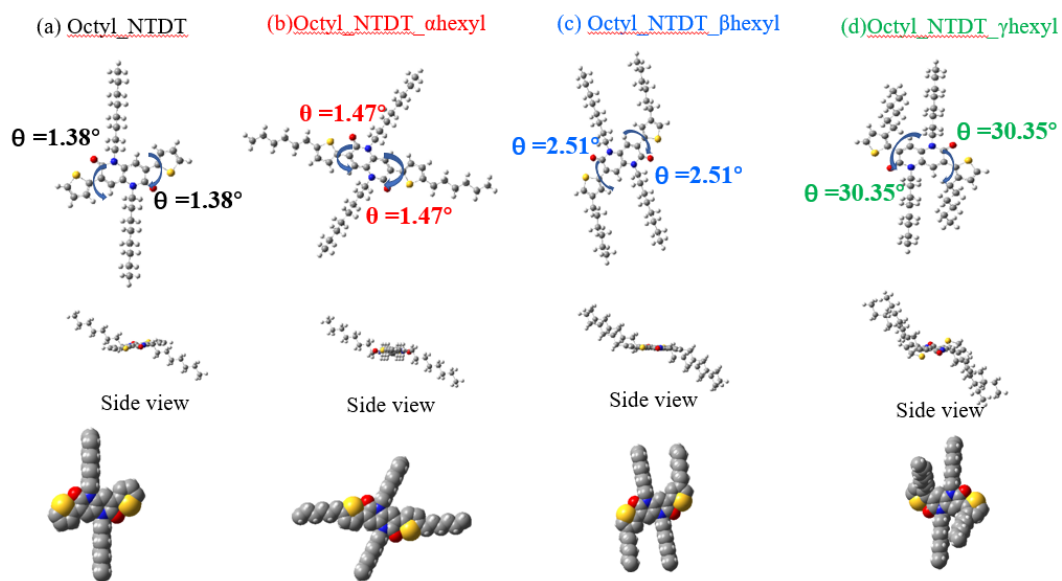
Figure 2. 2 The calculated geometry on ground state. Optimized geometries after calculation using basis set B3LYP/6-31G*. (Upper: Front view, Bottom: side view) (a) Octyl_NTDT, (b) Octyl_NTDT_αhexyl, (c) Octyl_NTDT_βhexyl, and (d) Octyl_NTDT_γhexyl .

2.3.2 Optical and electrochemical properties of NTD-based small molecules

Optical properties of target materials were investigated through UV-Vis spectra. **Figure 2. 3** showed the absorption spectra of the target molecules both in dichloromethane solution and in vapor deposited film. The fluorescence spectra both in solution and in solid state are also shown in **Figure 2. 4**. **Table 2. 1** summarized optical properties of NTD-based small molecules in solution and solid state.

The electrochemical properties were performed by cyclic voltammetry in both solution and solid state. CV was employed to investigate HOMO level of NTD derivatives for both solution state and solid state. HOMO level of each target material could be measured compared with ferrocene using as an internal standard (Fc$^+$/Fc = 4.8 eV) through the oxidation processes investigated by CV. The LUMO levels both in solution and solid state could be measured by the optical onset wavelength in UV/VIS spectroscopy and HOMO levels that were measured by CV. Electrochemical properties of NTD-based small molecules in solution and solid state were shown in **Figure 2. 8** and **Figure 2. 9.** A set of related data was summarized in **Table 2. 2** and **Table 2. 3.** And in order to express the relationship of energy levels in solid state and solution state compared with DFT calculation intuitionistically and vividly, all information in relation to electrochemical properties were exhibited in **Figure 2. 10**.

Figure 2. 3 (a) shows the normalized UV–vis absorption spectra of the target molecules in dichloromethane solution. The absorption spectra of Octyl_NTDT_αhexyl and Octyl_NTDT_βhexyl showed similar characteristics, whereas a small blue shift can be seen from Octyl_NTDT_γhexyl, which is in accordance with the molecular geometry shown in DFT calculation. This blue shift was regarded as a result of the geometry difference in planarity caused by steric hindrance of the hexyl chain pointing toward the NTD accepting unit. From the absorption spectra of target materials in solution state, we can confirm that there is little influence of changing the position of side chain on the optical band gap of these target molecules in solution. Octyl_NTDT, Octyl_NTDT_αhexyl, and Octyl_NTDT_βhexyl exhibited similar emission characteristics in solution except the slight blue shift of Octyl_NTDT_γhexyl due to its tilted structure (**Figure 2. 3 (b)).**

Interestingly, the photoluminescence quantum yields of NTDT derivatives in the solution state all emitted strong photoluminescence values (Φ_{PL}) as high as 100 % under UV light illumination regardless of the substitution of additional hexyl chains, which was considered as promising fluorescent materials. Surprisingly, Octyl_NTDT_γhexyl showed a high fluorescence even though it has a twisted structure after introducing additional alkyl chain (**Table 2. 1**).
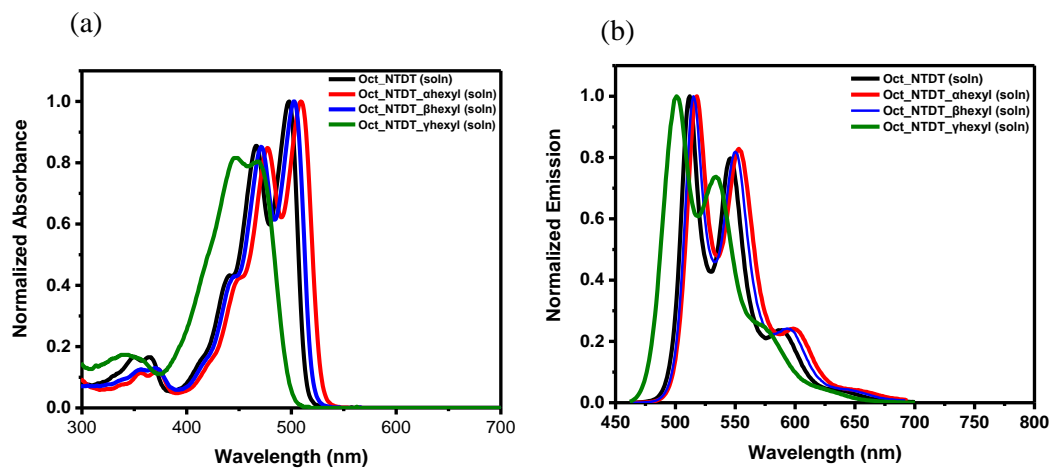
Figure 2. 3 (a) UV/Vis absorption spectra and (b) photoluminescence spectra for each derivative at solution state.
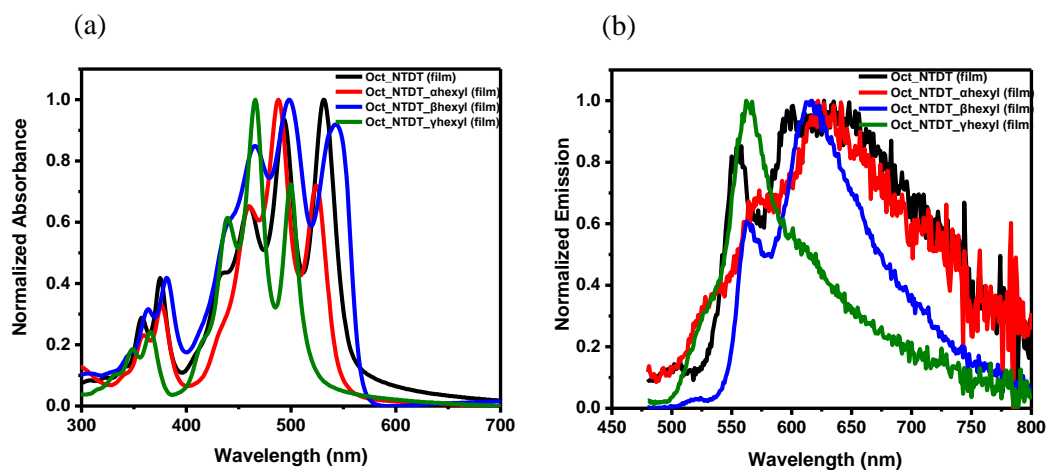

Figure 2. 4 (a) UV/Vis absorption spectra and (b) photoluminescence spectra for each derivative at solid state.

However, in solid state, self-assembly properties of target molecules induced changes in the optical absorption and emission that are quite different from isolated state. From film UV and PL spectra **(Figure 2.4)**, well-resolved vibronic structure with structured peaks appeared in the range of 450-550 nm, inferring that the change of molecular packing was able to be induced in solid state of target materials. [11] And as can be seen from **Figure 2. 4 (a),** NTD derivatives exhibited two typical strong absorption bands in solid state. The absorption peaks in the 450-550 nm range were due to the π-π transition of the conjugated backbone with strong intramolecular charge transfer (ICT) between electron donors (thiophene ring) and electron acceptor (NTD core). The maximum absorption was achieved in the range of 480-510 nm, and the shoulder peak at 350-400 nm was caused by local transition.

According to the result of PL in solid state, there are significant differences between Octyl_NTDT, Octyl_NTDT_αhexyl, Octyl_NTDT_βhexyl and Octyl_NTDT_γhexyl. From **Figure 2. 4 (b)** and **Figure 2. 6**, red-shifted mirror-like images could be seen from all target materials in the solid state, and they showed different intensities, indicating that NTDT derivatives have different molecular packing, which had an influence on the high-performance transistors.

Figure 2. 5 showed that UV/Vis absorption spectra of four target materials in solution state displays a mirror-like relationship with emission spectra.In addition, However, the fluorescence spectra in solid state of all NTD derivatives showed red shift compared to the spectra in solution.

Figure 2. 7 was taken to show the variation in the photoluminescence quantum yields (ΦPL) of the NTD derivatives under UV light illumination, ΦPL of NTDT derivatives in solution were detected which were excellent and unity regardless of the substitution of alkyl groups. While the thin films of target materials had different ΦPL values depending on the position of hexyl substitution.
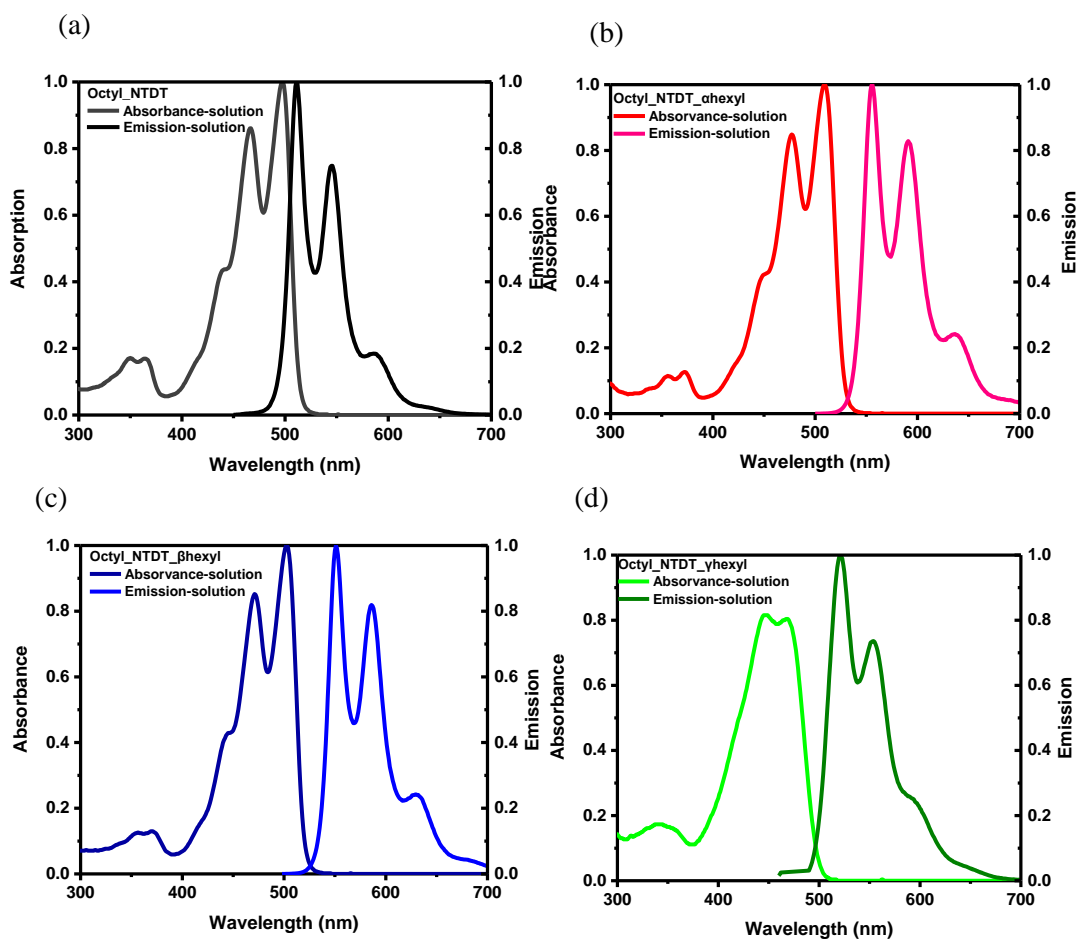
**Figure 2. 5** UV/Vis absorption spectra and Emission spectra of (a) Octyl_NTDT, (b) Octyl_NTDT_αhexyl, (c) Octyl_NTDT_βhexyl, and (d) Octyl_NTDT_γhexyl at solution state.
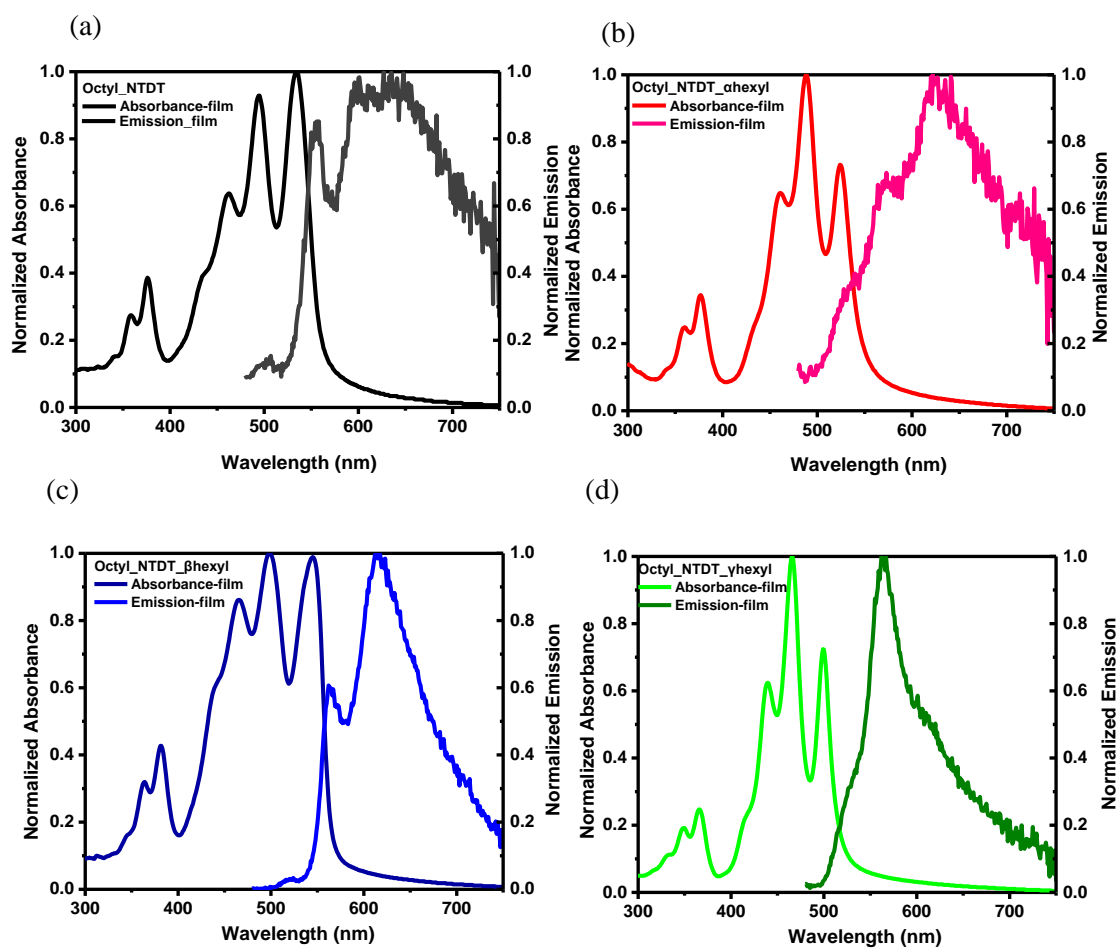
Figure 2. 6 UV/Vis absorption spectra and Emission spectra of (a) Octyl_NTDT, (b) Octyl_NTDT_αhexyl, (c) Octyl_NTDT_βhexyl, and (d) Octyl_NTDT_γhexyl at solid state

Table 2. 1 Optical properties of NTD-based small molecules in solution and solid state.

Compound	λ_{max}^{film} (nm)	λ_{onset} (nm)	$\lambda_g^{opt,}$ (eV)[a]	Φ_{PL} (%)
Octyl-NTDT (solu)[b]	498	516	2.40	100 [d]
Octyl-NTDT (film)[c]	534	565	2.19	NA [e]
Octyl-NTDT-αhexyl (solu) [b]	509	530	2.34	100 [d]
Octyl-NTDT-αhexyl (film)[c]	489	551	2.25	NA [e]
Octyl-NTDT-βhexyl (solu)[b]	503	522	2.37	100 [d]
Octyl-NTDT-βhexyl (film)[c]	498	570	2.17	3.88 [e]
Octyl-NTDT-γhexyl (solu)[b]	448	503	2.46	100 [d]
Octyl-NTDT-γhexyl (film)[c]	466	524	2.37	1.05 [e]

a) Optical band-gap energy was calculated from absorption onset point.

b) Measured in $CHCl_3$ solution of concentration of $2x10^{-3}$ M

c) Spin-coated with 10mg/ml concentration in $CHCl_3$ solution with filter syringe.

d) Relative PLQY, relative: quinine sulfate

e) Absolute PLQY
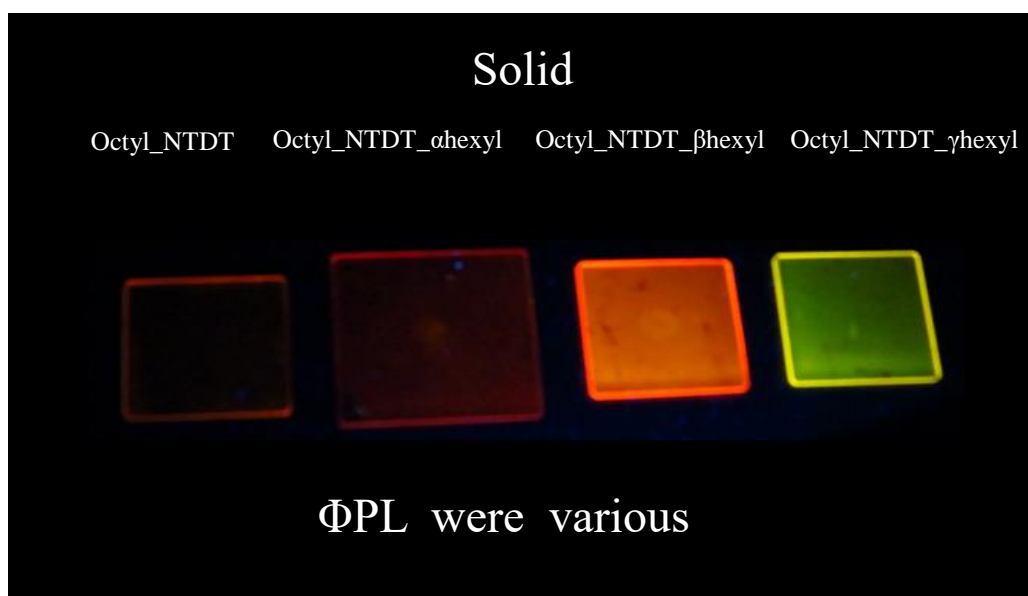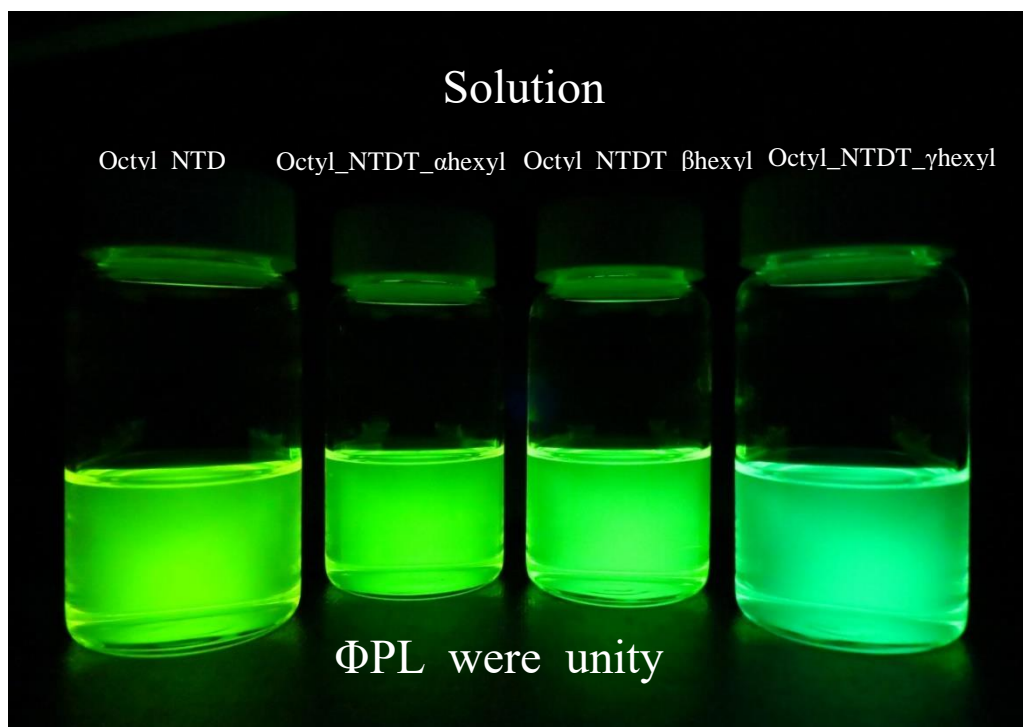
Figure 2. 7 Photograph taken to show the variation in the photoluminescence quantum yields (ΦPL) of the NTD derivatives under UV light illumination.in (a) Solution state ; (b) Solid state.

CV as an important technique was employed to investigate HOMO level of NTD derivatives for both solution state and solid state, which provides a reference for device test. Organic semiconductors using in OFET are required to have proper molecular energy level to satisfy carrier injection and characteristics, so as to achieve the best performance in transistors. For p-type semiconductors, HOMO level should be in the range of -5.0 eV to -5.5 eV for hole injection matching with Au electrode. [14] So, I ascertained HOMO levels of NTD derivatives in solid state before device test.

From the film CV results, it was confirmed that the HOMO levels of target materials that were estimated by the onset of oxidation process become deeper gradually in solid state. The energy levels of NTD series in solid state are listed in **Table 2. 2**. The Octyl_NTDT_γhexyl had the lowest HOMO level (HOMO: -5.71 eV) among these NTD-based molecules, presumably due to the relatively disordered packing structure of the thin film caused by the static hindrance induced by the position of side chains. [15] The lowest HOMO level of Octyl_NTDT_γhexyl was regarded to be harmful to the carrier injection and transistor performance. While Octyl_NTDT_αhexyl involving π-conjugation showed the highest HOMO level due to the strong intermolecular interaction,which was regarded as a promising p-type organic semiconductor for transistors because p-type molecules used in transistors always have high HOMO levels with good electron-donating properties. [13] From the analysis of film CV results,the significant difference in energy level suggested the fact that intermolecular interaction of Target molecules in solid state is different. So, changing the position of substituted alkyl chains can exert its influence on self-assembled properties through tuning the static the steric hindrance effect, which is correlated well with my research objective.

Detailed solution CV results are shown in **Table 2. 3.** There are slight difference in HOMO energy levels at Octyl_NTDT, Octyl_NTDT_αhexyl, Octyl_NTDT_βhexyl, and Octyl_NTDT_γhexyl, consistent with the results of DFT calculation.
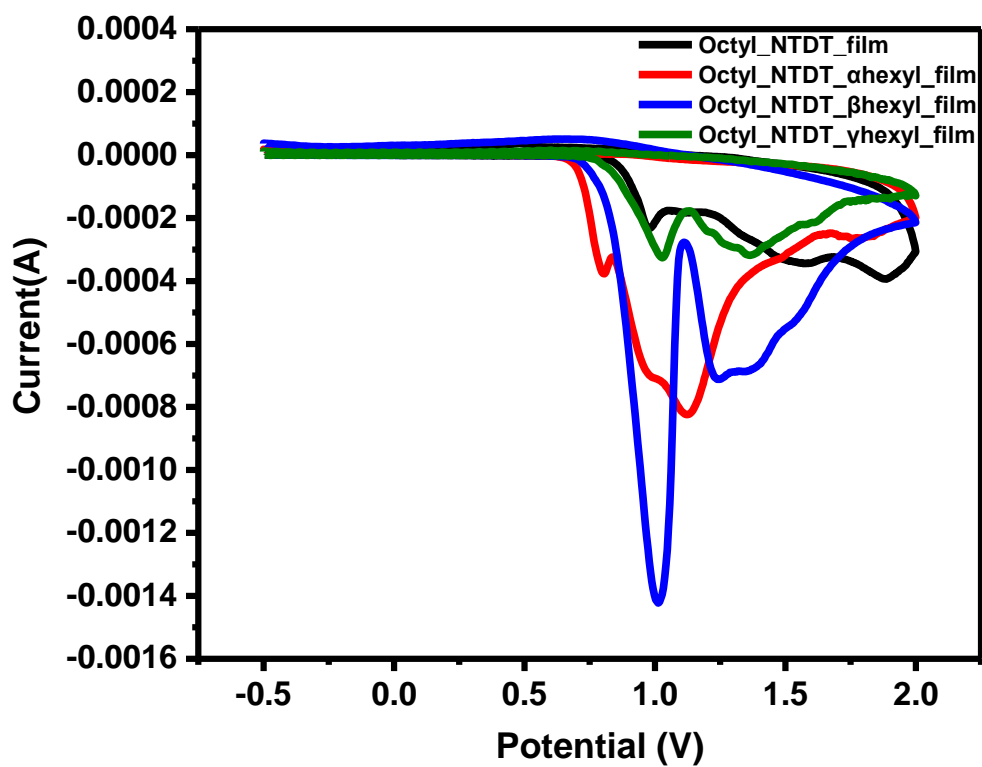
Figure 2. 8 Cyclic voltammetrams NTD-based derivatives in film state. (a) Octyl_NTDT, (b) Octyl_NTDT_αhexyl, (c) Octyl_NTDT_βhexyl, and (d) Octyl_NTDT_γhexyl. All were vapor deposited on quartz and supporting electrolyte was TBAHFB in acetonitrile (ACN). Ferrocene (filled) with TBAHFB in ACN solution as the reference.

Table 2. 2 Electrochemical properties and energy levels of NTD-based derivatives in film states.

Compound	E_{HOMO} (eV)[a]	E_{LUMO*} (eV)[b]	$E_g^{opt,film}$ (eV)[c]
Octyl-NTDT	5.37	3.17	2.19
Octyl-NTDT-αhexyl	5.33	3.08	2.25
Octyl-NTDT-βhexyl	5.45	3.28	2.17
Octyl-NTDT-γhexyl	5.72	3.35	2.37

a) Electrochemical HOMO level is recorded by cyclic voltammetry. It calculated from difference between ferrocene reference (-4.8 eV) and each material.

b) LUMO level is calculated with measured electrochemical HOMO and optical bandgap.

c) Optical bandgap was calculated by absorption onset.
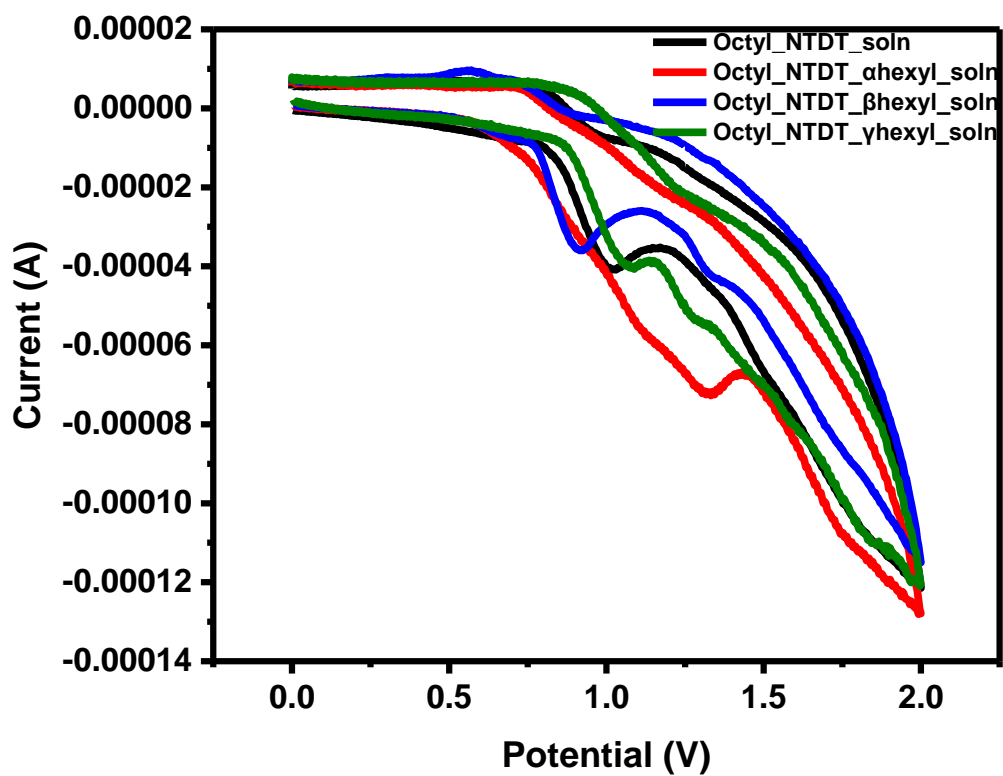
Figure 2. 9 Cyclic voltammetrams NTD-based derivatives in solution   state. (a) Octyl_NTDT, (b) Octyl_NTDT_αhexyl, (c) Octyl_NTDT_βhexyl,and (d) Octyl_NTDT _γhexyl . At solution state, supporting electrolyte was TBATFB methylene chloride (MC).

Table 2. 3 Electrochemical properties and energy levels of NTD-based derivatives in solution states.

Compound	E_{HOMO} (eV)[a]	E_{LUMO*} (eV)[b]	$E_g^{opt,film}$ (eV)[c]
Octyl-NTDT	5.39	2.99	2.40
Octyl-NTDT-αhexyl	5.24	2.90	2.34
Octyl-NTDT-βhexyl	5.32	2.95	2.37
Octyl-NTDT-γhexyl	5.44	2.98	2.46

a) Electrochemical HOMO level is recorded by cyclic voltammetry. It calculated from difference between ferrocene reference (-4.8 eV) and each materials.

b) LUMO level is calculated with electrochemical HOMO and optical bandgap.

c) Optical bandgap was obtained by onset of absorption.
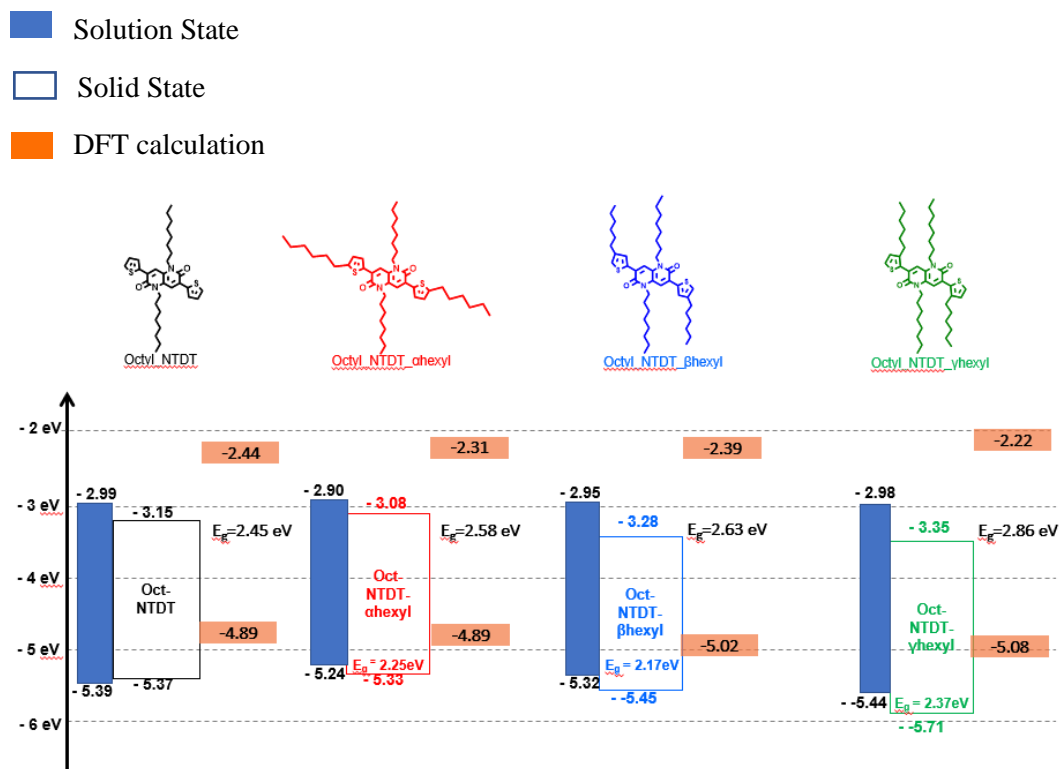
Figure 2. 10 Electrochemical properties and energy levels of NTD-based derivatives in solid state, solution states, and DFT calculation.

2.3.3 Thermal stability of molecules of NTD-based small molecules

Melting points of NTD derivatives are available from differential scanning calorimetry (DSC). 5 mg of each material was weighed, and then DSC was performed from 20 °C to 350 °C. at 10 ºC/min heating rate in nitrogen atmosphere. As shown in **Figure 2. 11**, target substances with the same molecular weight have different melting points,deduced that they have different molecular packing structures. Due to the static hindrance, Octyl_NTDT_γhexyl (T_m = 128.6°C) exhibited lower thermal degradation temperature than Octyl_NTDT_αhexyl (T_m = 168.3°C) and Oct_NTDT_βhexyl (T_m = 188.3°C). Octyl_NTDT_αhexyl and Octyl_NTDT_βhexyl showed a higher melting point, which indicated that molecules are tightly packed together with stronger intermolecular interaction, leading to the improvement of charge carrier mobility in transistors.

From the TGA results, we can clearly obtain the decomposition temperature of the compounds. As shown in **Figure 2. 12**, the TGA study indicates that all NTD derivatives possess excellent thermal stability in nitrogen atmosphere with a decomposition temperature (T_d, 5% weight loss) of 362.5 °C for Octyl_NTDT_αhexyl, and 354.9 °C for Octyl_NTDT_βhexyl, and 312.6 °C for Octyl_NTDT_γhexyl which is high enough for applications of these materials in OFETs.
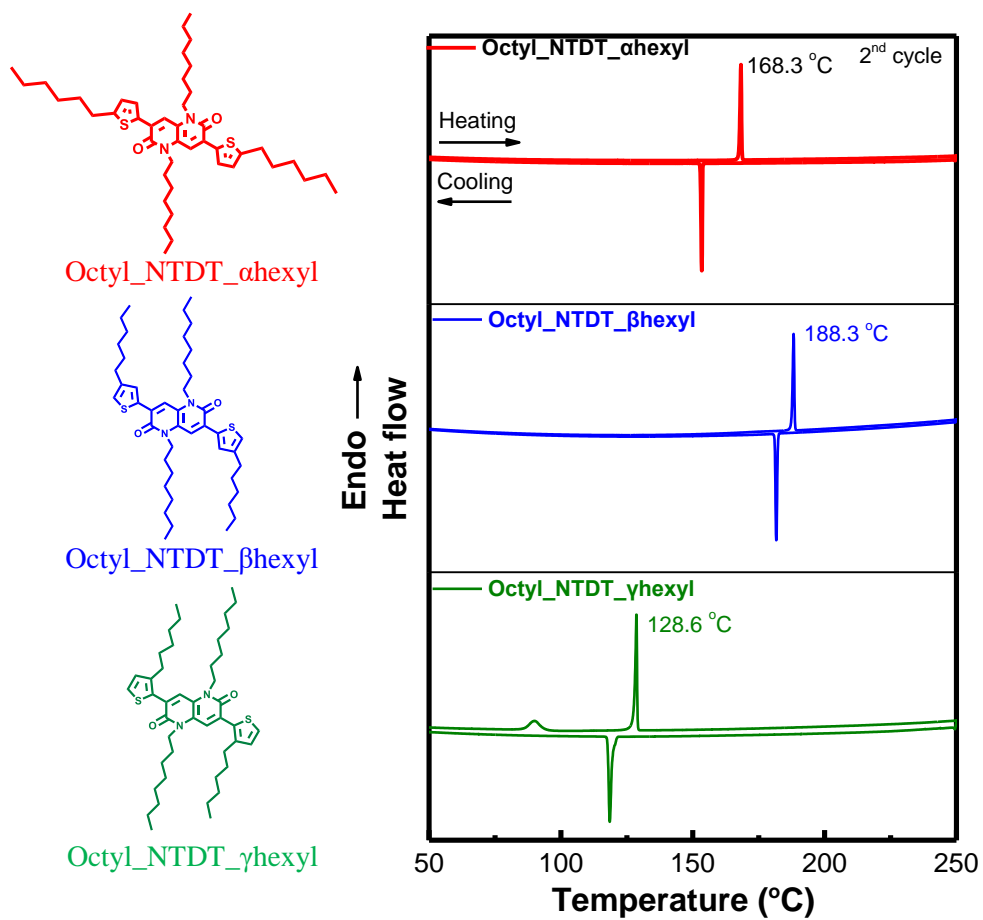
**Figure 2. 11** DSC trace of the (a) Octyl_NTDT_αhexyl, (b) Octyl_NTDT_βhexyl, and (c) Octyl_NTDT_γhexyl.
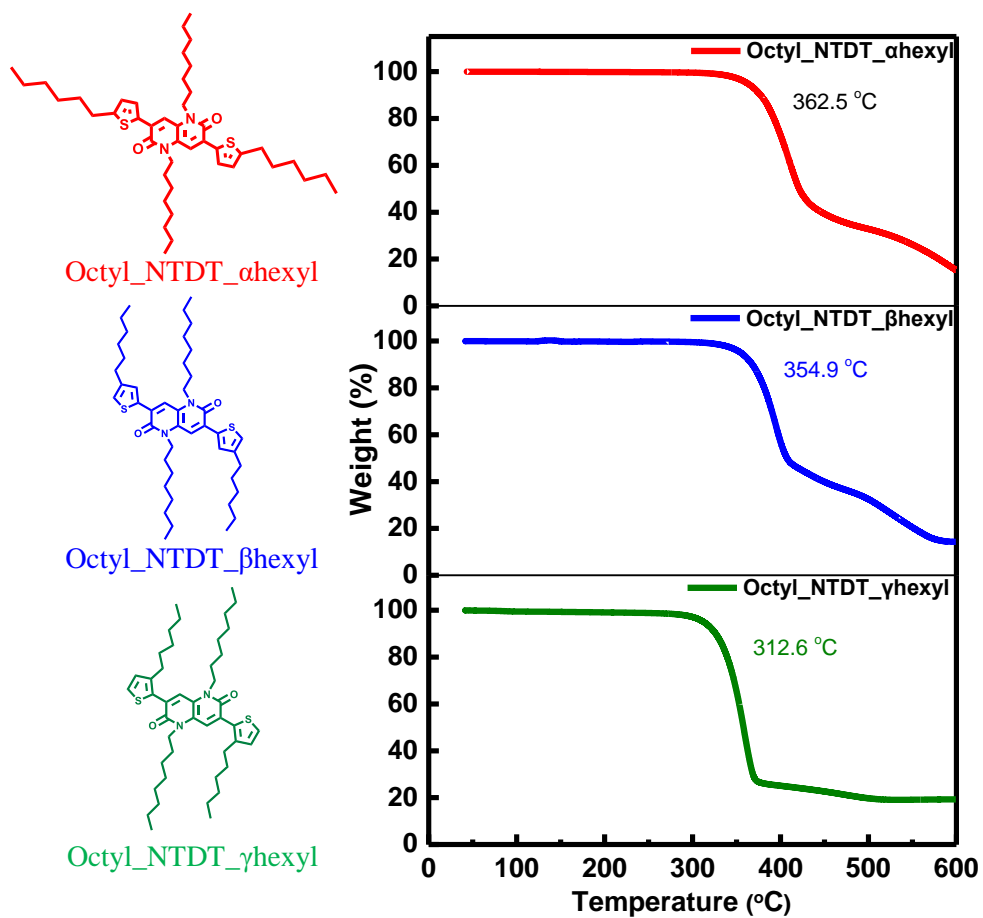
Figure 2. 12 TGA analysis of molecules for checking thermal stability. Increase of temperature is 10 ℃/min and range of temperature is 600 ℃.

2.3.4 Vacuum deposited OFETs performance

The device performance test was conducted based on the bottom-gate device structure using gold electrode by vapor deposited method. In order to reduce the influence of surface defects and enhance the ordering of molecular arrangement, we adopt n-octadecyltrimethoxysilane (ODTS) self-assembled SiO_2/Si substrates during vapor deposited process. As can be seen from the output curve and transfer curve **(Figure 2. 13)**, the typical p-type characteristics were displayed at optimum annealing conditions. OFET characteristics of Octyl_NTDT_αhexyl, Octyl_NTDT_βhexyl, and Octyl_NTDT_γhexyl based on vacuum deposited process were outlined in **Table 2. 4.**

At room temperature, Octyl_NTDT_αhexyl gave average hole mobility of 7.25×10^{-2} $cm^2\,V^{-1}\,s^{-1}$, whereas Octyl_NTDT_γhexyl gave an average value of $6.27\times10^{-3}\,cm^2\,V^{-1}\,s^{-1}$, which is 1 order of magnitude lower. So, it is absolute that changing the position of alkyl solubilizing substituents could exert its considerable influence on carrier mobilities through tuning the steric hindrance effect. After increasing the annealing temperature to 70 °C, maximum mobility of $0.44\,cm^2\,V^{-1}\,s^{-1}$ at Octyl_NTDT_αhexyl was measured. The highest performance of Octyl_NTDT_αhexyl was exhibited on annealing temperature at 70 ℃ whereas other small molecules showed optimal charge carrier mobilities at 110 ℃. From the obtained p-type OFET characteristics, it is clear that the features of the position of alkyl chain attached to the nitrogen atoms of lactam group have an appreciable impact on charge carrier transport

According to previous research, thiophene flanked DPP core exhibits maximum hole mobility of $2.7\times10^{-2}\,cm^2\,V^{-1}\,s^{-1}$, [16] Upon comparing the obtained carrier mobility results for our newly reported Octyl_NTDT derivatives in this work with that of previously reported DPP core substituted by thiophene, our NTD-based small molecules exhibit charge carrier mobility in 10^{-1} level which is one orders of magnitude higher than DPP substituted by thiophene, indicating that NTD-based small molecule is a highly promising candidate p-type semiconductors for transistors. [17]

In order to evaluate the performance of NTD derivatives, optical microscopy (OM) was performed. As shown in **Figure 2. 14,** the large crystals existed two-dimensional layer

by layer growth with 2D layered terrace structure, which is beneficial for high-performance transistors. With rising of annealing temperature, grain size became bigger during reductive annealing process, which is helpful for the charge transport.
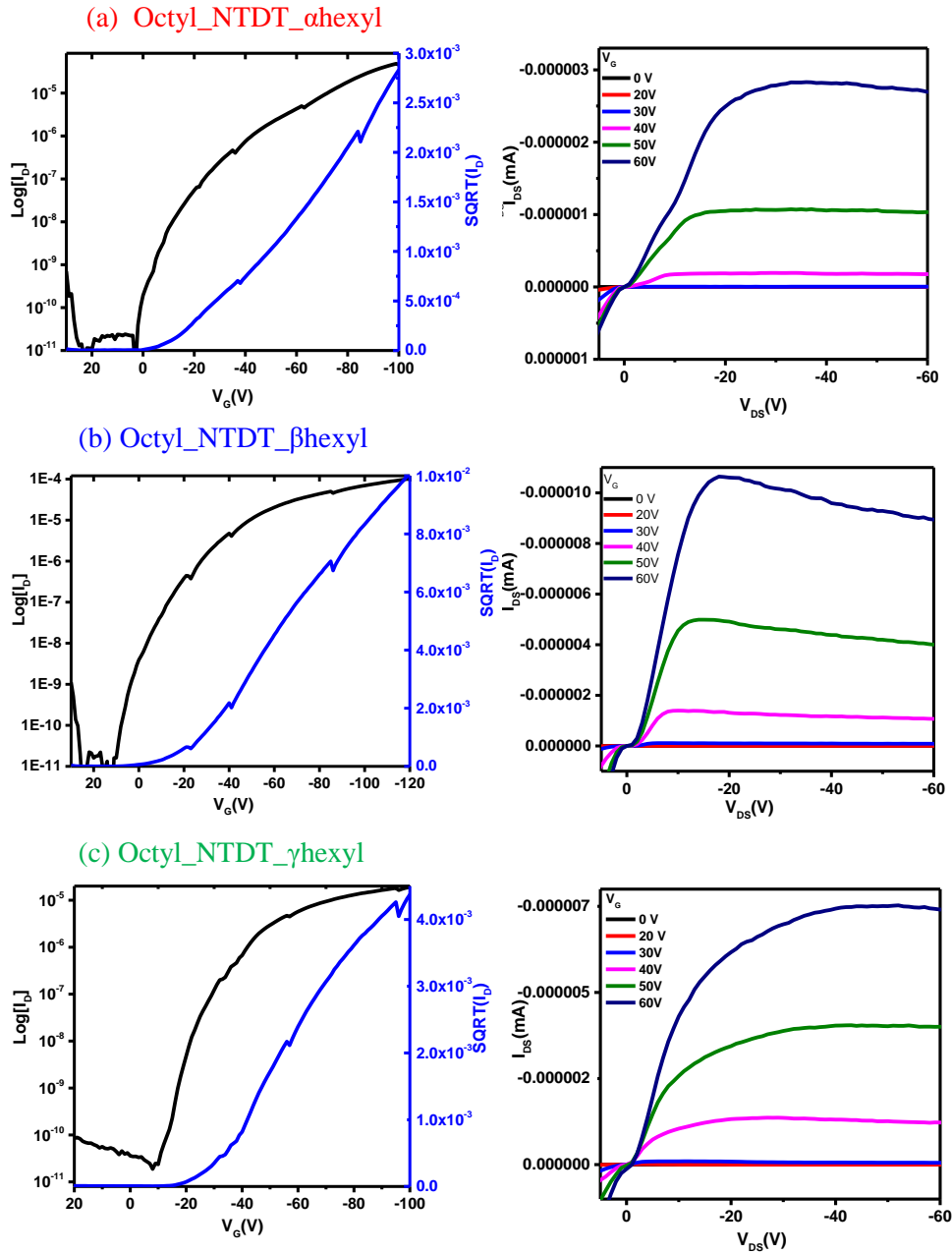
Figure 2. 13 Transfer and output curves of vacuum deposited (a) Octyl_NTDT_αhexyl, (b) Octyl_NTDT_βhexyl, and (c) Octyl_NTDT_γhexyl films.

Table 2. 4 OFET characteristics of (a) Octyl_NTDT_αhexyl, (b) Octyl_NTDT_βhexyl, and (c) Octyl_NTDT_γhexyl based on vacuum deposited process.

Compound	T_{sub}	$\mu_{h,avg}$ (cm^2/Vs)	$\mu_{h,max}$ (cm^2/Vs)	V_{Th} (V)	Log (I_{on}/I_{off})
Octyl_NTDT_αhexyl	25 ℃	3.07×10^{-2}	7.25×10^{-2}	-34.7	6.0
	70 ℃	2.59×10^{-1}	4.38×10^{-1}	-49.9	6.9
	110 ℃	8.83×10^{-2}	1.51×10^{-1}	-19.9	6.9
Octyl_NTDT_βhexyl	25 ℃	1.89×10^{-2}	3.94×10^{-2}	-43.9	5.8
	70 ℃	8.62×10^{-2}	1.59×10^{-1}	-17.7	7.0
	110 ℃	1.36×10^{-1}	2.38×10^{-1}	-16.4	7.0
Octyl_NTDT_γhexyl	25 ℃	6.27×10^{-3}	6.27×10^{-3}	-66.7	4.7
	70 ℃	4.06×10^{-2}	5.30×10^{-2}	-25.5	6.0
	110 ℃	6.80×10^{-2}	1.34×10^{-1}	-29.7	5.7

Figure 2. 14 OM images of the thin films: for (a) Octyl_NTDT_αhexyl, (b) Octyl_NTDT_βhexyl, and (c) Octyl_NTDT_γhexyl at RT, 70 °C, and 110 °C, respectively. Scale bars for OM images are 20 μm,

2.3.5 XRD and GIWAX analysis of Vacuum deposited film

As shown in the diffractogram of the vapor-deposited film (**Figure 2. 15**), there are clear diffraction peaks arising from π-π plane stacking distance. And out of plane lattice parameters from thin film for three target materials were outlined in **Table 2. 5**. For Octyl_NTDT_αhexyl that exhibited best OFET performance, highest resolved shark diffraction peaks at annealing temperature 70° were observed at $2\Theta = 4.45°$ (d (001) = 19.84 Å), 8.85°, 13.29°, which indicated that the Octyl_NTDT_αhexyl molecule exhibit well-organized intermolecular ordering, resulted in the enhanced crystallinity. However, it is difficult to find highly ordered and obvious diffraction peak even after annealing temperature at 110°C in Octyl_NTDT_γhexyl molecule, which is one of the reasons why it exhibited the lowest charge mobility among them. And according to Scherrer equation, crystallite sizes could be obtained. Vapor deposited Octyl_NTDT_αhexyl had larger crystallites than those of other thin films, which is advantageous for the charge carrier transport in transistors.

The XRD results are in agreement with viewpoint that the hexyl substituent can greatly affect the packing orientation of molecules in the solid state, which could have an influence on molecular orbital overlap and the π-electron delocalization and thus resulted in the changes of energy levels in solid state. [18]

GIWAXS parameters were summarized in **Table 2. 6**. According to the analysis of the GIWAXS data for all vapor deposited films **(Figure 2. 16)**, well-pronounced diffraction spots occurred in Octyl_NTDT_αhexyl and Octyl_NTDT_βhexyl, indicating that thin-films of these two materials have a crystalline nature. While the GIWAX pattern of the Octyl_NTDT_γhexyl thin-film exhibited weak and indistinct of relatively lower crystallinity, which is consistent with the XRD results.

To sum up, through the analysis of the experimental data, there are mainly two reasons to explain the OFET performance. On the one hand, Octyl_NTDT_γhexyl have a larger tilting angle than other materials resulting in a less planar geometry with unfavorable steric hindrance and leading to weak intermolecular interactions with adjacent conjugated subunits, [19] further caused the loose molecular packing and cavities in the crystalline, …
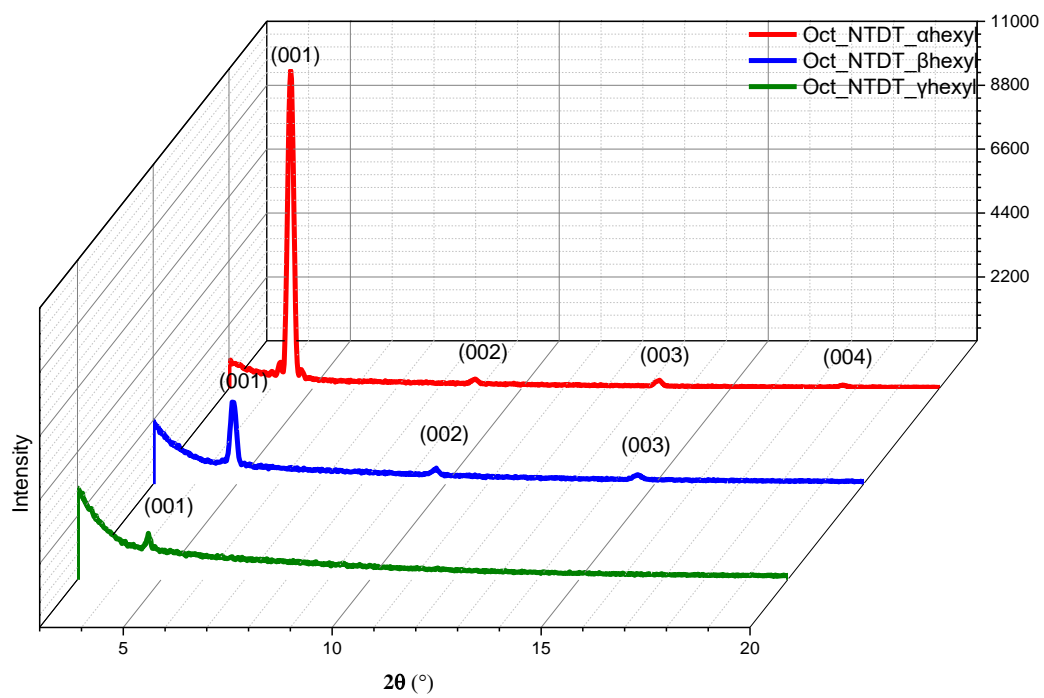
Figure 2. 15 Out of plane XRD of images (a) Octyl_NTDT_αhexyl, (b) Octyl_NTDT_βhexyl, and (c) Octyl_NTDT_γhexyl as vapor deposited film

Table 2. 5 Out of plane lattice parameters from thin film for (a) Octyl_NTDT_αhexyl, (b) Octyl_NTDT_βhexyl, and (c) Octyl_NTDT_γhexyl.

Small molecule	001	002	003	Out of plane d-spacing [Å]	FWHM	Crystalite size [Å][a)]
Oct-NTDT_αhexyl	4.45	8.85	13.29	19.84	0.154	573
Oct-NTDT_βhexyl	4.87	9.67	14.52	18.13	0..167	529
Oct-NTDT_γhexyl	4.79			18.43	0.203	436

(a) Crystalite size could be measured by Scherrer equation [23]:

$$L = 0.90\lambda / (FWHM \cdot \cos\theta)$$

(L: average crystallite size, λ: X-ray wavelength, FWHM: peak width at half-maximum intensity, 0.90: Scherrer constant) [23]
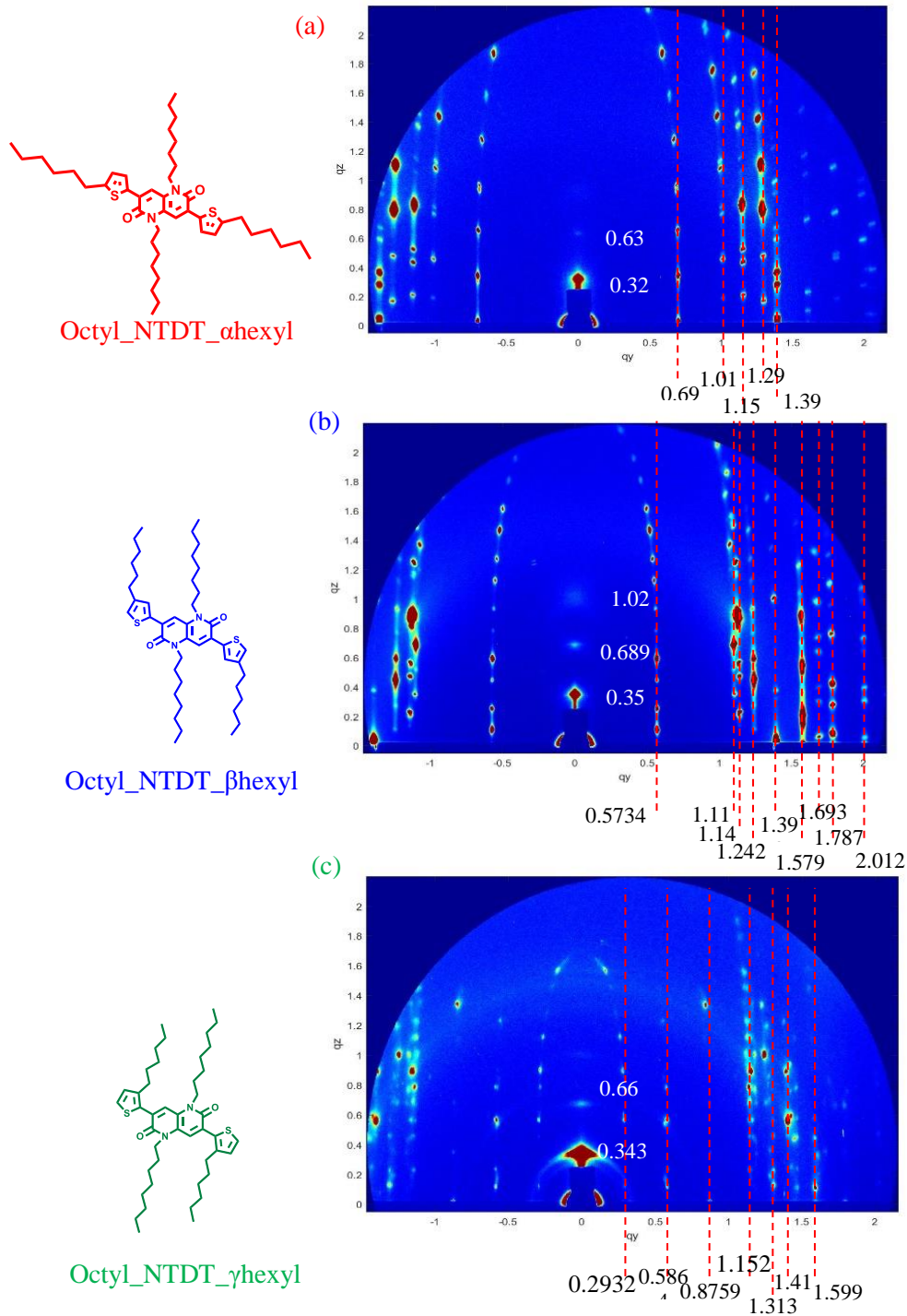
Figure 2. 16 Two-dimensional GIWAXS images of (a) Octyl_NTDT_αhexyl, (b) Octyl_NTDT_βhexyl, and (c) Octyl_NTDT_γhexyl as vapor deposited film at 110°.

Table 2. 6 Two-dimensional GIWAXS parameters of (a) Octyl_NTDT_αhexyl, (b) Octyl_NTDT_βhexyl, and (c) Octyl_NTDT_γhexyl at 110° in vapor deposited transistors.

Small molecules	Annealing Temperature	Lamellar spacing	
		Scattering vector (q) [Å^{-1}]	d-spacing [Å]
Oct-NTDT-αhexyl	110℃	0.32	19.63
Oct-NTDT-βhexyl	110℃	0.35	17.94
Oct-NTDT-γhexyl	110℃	0.667	18.31

2.3.6 Solution process OFETs performance

At present, many small molecules have poor solubility, and the molecular weight is too small, resulting in a low viscosity of the solution, which is difficult to process into a film by solution processing.

In order to solve the issue, it's accepted that attaching alkyl chains endowed with solubility can not only improve solution-processability of semiconducting molecules but also have a considerable impact on controlling self-assembly properties. Here, organic field effect transistors (OFET) using solution processed technique based on NTD series small molecules with bottom-gate device structure using gold electrode.

For Octyl_NTDT_αhexyl and Octyl_NTDT_βhexyl, it's clearly seen from the p-type output curve **(Figure 2. 17)**, the good saturation characteristics were shown in the curve as the V_G voltages were rising, and the current and voltage shown relative linearity under low voltage, which indicated that HOMO levels of these molecules match well with gold work function, leading the charge carrier mobility is less hindered due to the barrier is smaller. OFET characteristics of Octyl_NTDT_αhexyl, Octyl_NTDT_βhexyl, and Octyl_NTDT_γhexyl based on spin-coating process were outlined in **Table 2. 7.** After optimizing performance, the optimized performance of Octyl_NTDT_αhexyl was exhibited on annealing temperature at 70 ℃ whereas other small molecules showed optimal charge carrier mobilities at 110 ℃. After annealing, Octyl_NTDT_βhexyl exhibited the highest hole mobility of 9.11×10^{-2} cm^2 V^{-1}s^{-1}.

(b) Octyl_NTDT_αhexyl


(b) Octyl_NTDT_βhexyl
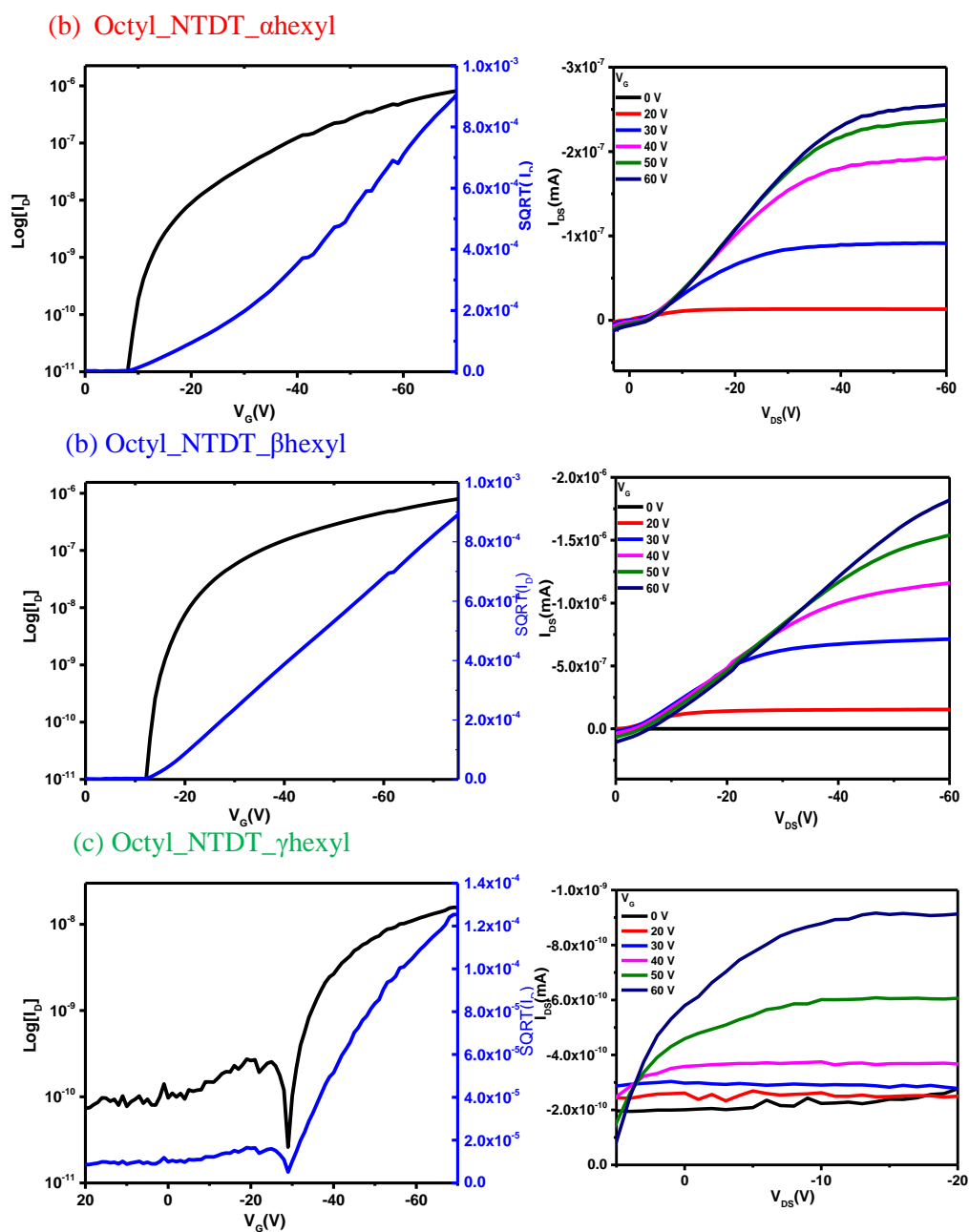
(c) Octyl_NTDT_γhexyl

Figure 2. 17 Transfer and output curves of spin-coating (a) Octyl_NTDT_αhexyl, (b) Octyl_NTDT_βhexyl, and (c) Octyl_NTDT_γhexyl films.

Table 2. 7 OFET characteristics of (a) Octyl_NTDT_αhexyl, (b) Octyl_NTDT_βhexyl, and (c) Octyl_NTDT_γhexyl based on solution process process.

Compound	$T^{a)}_{sub}$	$\mu_{h,avg}$ (cm^2/Vs)	$\mu_{h,max}$ (cm^2/Vs)	V_{Th} (V)	Log (I_{on}/I_{off})
Octyl_NTDT_αhexyl	25 ℃	3.31×10^{-3}	5.06×10^{-3}	-39.2	5.0
	70 ℃	5.42×10^{-3}	7.14×10^{-3}	-13.7	4.0
	110 ℃	4.27×10^{-3}	4.93×10^{-3}	-9.3	4.0
Octyl_NTDT_βhexyl	25 ℃	3.59×10^{-5}	8.41×10^{-5}	-16.9	3.0
	70 ℃	1.70×10^{-3}	4.21×10^{-3}	-8.8	6.0
	110 ℃	3.57×10^{-2}	9.11×10^{-2}	-11.1	6.0
Octyl_NTDT_γhexyl	25 ℃	4.04×10^{-5}	2.18×10^{-4}	-43.1	2.8
	70 ℃	6.02×10^{-6}	2.00×10^{-5}	-54.7	2.0
	110 ℃	6.88×10^{-5}	2.45×10^{-4}	-27.9	2.5

(a) The spin-coated film was annealed at 70 °C, 110 °C for 10 min, respectively.

2.3.7 XRD analysis for Solution processed OFETs

In order to evaluate the performance of NTD derivatives,out-of-plane XRD was performed. As shown in **Figure 2. 18,** spin-coated films of all materials exhibited sharp and clear diffraction peaks at 2θ = 4.45°, 4.89°, and 4.71° for Octyl_NTDT_αhexyl, Octyl_NTDT_βhexyl, and Octyl_NTDT_γhexyl, respectively, corresponding to an intermolecular lamellar distance of 19.84 Å, 18.06 Å, 18.74 Å, respectively. And according to Scherrer equation, Octyl_NTDT_βhexyl showed bigger crystallites size than those of other thin films, which is advantageous for the charge carrier transport in field effect transistors.
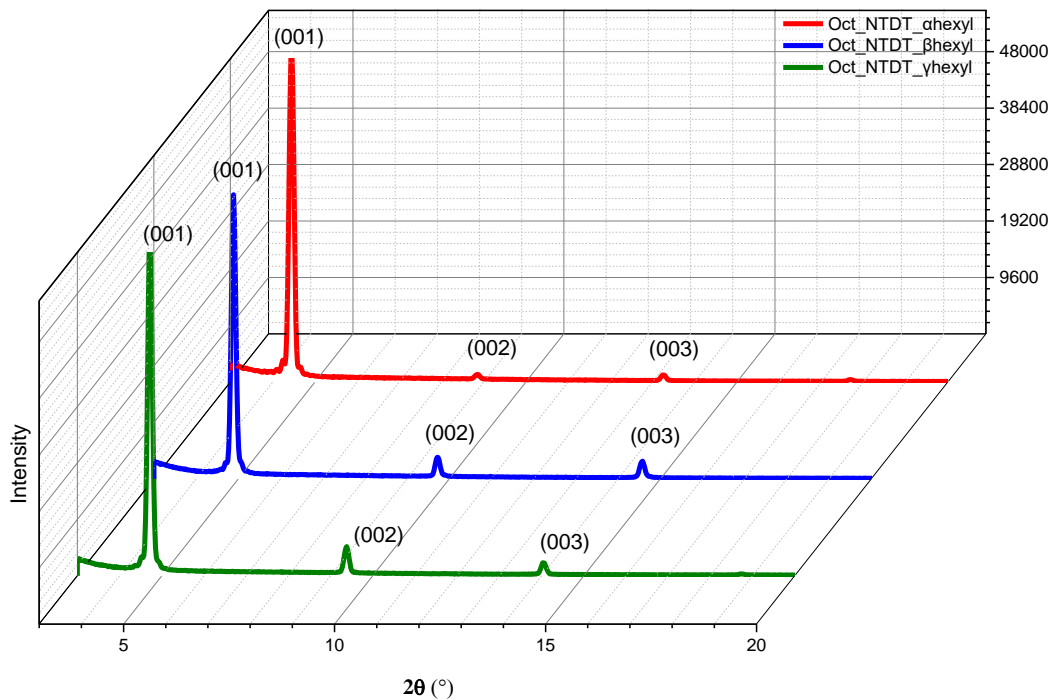
Figure 2. 18 Out of plane XRD of images (a) Octyl_NTDT_αhexyl, (b) Octyl_NTDT_βhexyl, and (c) Octyl_NTDT_γhexyl as spin-coating film

Table 2. 8 Out of plane lattice parameters from spin-coated thin film for (a) Octyl_NTDT_αhexyl, (b) Octyl_NTDT_βhexyl, and (c) Octyl_NTDT_γhexyl .

Small molecule	001	002	003	Out of plane d-spacing [Å]	FWHM	Crystalite size [Å][a)]
Oct-NTDT_αhexyl	4.45	8.86	13.26	19.84	0.125	706
Oct-NTDT_βhexyl	4.89	9.72	14.58	18.06	0.124	715
Oct-NTDT_γhexyl	4.71	9.38	14.03	18.74	0.128	689

(a) Crystalite size could be measured by Scherrer equation [23]:

$$L = 0.90\lambda/(FWHM \cdot \cos\theta)$$

(L: average crystallite size, λ: X-ray wavelength, FWHM: peak width at half-maximum intensity, 0.90: Scherrer constant) [23]

2.4. Conclusion

A systematic study of the structure-property relationship about π-conjugated molecules based on NTDT substituted with hexyl side chains at three different positions in the thiophene rings has been made for use in organic field effect transistor in different processing.

Firstly, I designed and synthesized a series of 1,5-naphthyridine-2,6-dione (NTD) acceptor-based conjugated molecules for OFETs, by differing in the thiophene of alkyl chain position. Then, all target materials were characterized by UV/Vis, CV, and DFT calculation, etc. It is found that changing the position of alkyl chains without electronic effect can exert its influence on the planarity and self-assembly properties. Through TGA analysis, all target materials showed high thermal stabilities, which is high enough for applications of these materials in OFETs.

P-type vapor deposited OFET device fabrications were progressed and Octyl_NTDT_αhexyl with high crystallinity showed the best performance for p-type and max mobility was $\mu_h = 0.44$ cm^2 V^{-1} s^{-1}. OM images showed two-dimensional well-connected morphology of vapor deposited film. In addition, organic field effect transistors (OFET) using solution processed technique based on NTD series small molecules were also fabricated, and maximum hole mobility of 9.11×10^{-2} cm^2 V^{-1} s^{-1} was achieved after annealing. From the obtained p-type OFET characteristics, it is clear that there was a correlation between the substitution position and device performance of the NTDT derivatives in both vacuum- and solution-processed OFET devices.

2.5. Bibliography

[1] D. G. Farnum, G. Mehta, G. G. I. Moore and F. P. Siegel, *Tetrahedron Lett.*, **1974**, 29, 2549

[2] Catherine Kanimozhi, Mallari Naik, Nir Yaacobi-Gross, Edmund K. Burnett, Alejandro L. Briseno, Thomas D. Anthopoulos, Satish Patil, *J. Phys. Chem. C,* **2014**, 118, 22.

[3] Palai. A, Cho. H, Cho.S, Shin. T, Jang. S, *Organic Electronics,* **2013**, 14, 1396-1406.

[4] Tantiwiwat. M, Tamayo, A,Luu. N, Dang, X. D, Nguyen, T.Q.,*Journal of Physical Chemistry C,* **2008,** 112, 17402-17407.

[5] Jae-Yoon Shin, Kil Suk Kim, Min-Chul Yoon, Jong-Min Lim, Zin Seok Yoon, Atsuhiro Osuka, Dongho Kim, *Chem. Soc. Rev.*, **2010**, 39, 2751-2767.

[6] Sung Cho, Zin Seok Yoon, Suk Kim, Min-Chul Yoon, Dong-Gyu Cho, Jonathan L. Sessler, Dongho Kim, *J. Phys. Chem. Lett.*, **2010**, 1, 6, 895-900.

[7] Jin-Hong Kim, Min-Woo Choi, Won Sik Yoon, Sangyoon Oh, Seung Hwa Hong, Soo Young Park, *ACS Appl. Mater. Interfaces.,* **2019**, 11, 8, 8301-8309.

[8] Won Sik Yoon, Dong-Won Kim, Jun-Mo Park, Illhun Cho, Oh Kyu Kwon, Dong Ryeol Whang, Jin Hong Kim, Jung-Hwa Park, Soo Young Park, *Macromolecules,* **2016**, 49, 22, 8489–8497.

[9] Won Sik Yoon,Dong-Won Kim, Min-Woo Choi, Jun-Mo Park, Soo Young Park, *Adv. Energy Mater.*, **2018**, 8, 1701467.

[10] Bisri S Z, Takenobu T, Takahashi T, et al., *Appl Phys Lett*, **2010**, 96, 18, 90-98.

[11] AlánAspuru-Guzikb, Niyazi Serdar Sariciftcia et al., *Organic Electronics*, **2014**, 15, 3521–3528.

[12] Jaehyun Lee, Hyo-Cheol Jung, Hwangyu Shin, Joonghan Kim, Daisuke Yokoyama, Hidetaka Nishimura, Atsushi Wakamiya, *J. Mater. Chem. C,* **2016**, 4, 2784-2792.

[13] Ki-Hyun Kim, Hojeong Yu, Hyunbum Kang, Dong Jin Kang, Chul-Hee Cho, Han-Hee Cho, Joon Hak Oh, *J. Mater. Chem. A*, **2013**, 1, 14538-14547.

[14] Alessandra Operamolla, Gianluca M. Farinola, Eur. *J. Org. Chem.*, **2011**, 423–450.

[15] Ting Lei, Jie-Yu Wang, Jian Pei, *Chem. Mater.* **2014**, 26, 1, 594-603.

[16] Jin-Hong Kim, Min-Woo Choi, Won Sik Yoon, Sangyoon Oh, Seung Hwa Hong, Soo

Young Park, *ACS Appl. Mater. Interfaces.*, **2019**, 11, 8, 8301-8309.

[17] Gabriela Wiosna-Salyga, Monika Gorab, Malgorzata Zagorska, Petr Tomand, Beata Luszczynskaa, Jiri Pflegerd, Ireneusz Glowackia, Jacek Ulanskia, Jozef Mieczkowskib, *RSC Adv.*, **2015**, 5, 59616-59629.

[18] Tadeusz Marek Krygowski, Beata Tamara Stępień, *Chem. Rev.,* **2005**, 105, 10, 3482-3512

[19] M. A. Naik, N. Venkatramaiah, C. Kanimozhi, S. Patil, J. Phys. Chem. C, 2012, 116, 26128.

[20] Can Wang, Zhen Li, Mater, *Chem. Front*., **2017**, 1, 2174-2194.

[21] C. D. Dimitrakopoulos and P. R. L. Malenfant, *Adv. Mater.*, **2002**, 14, 99.

[22] A. C. Mayer, M. F. Toney, S. R. Scully, J. Rivnay, C. J. Brabec, M. Scharber, M. Koppe, M. Heeney, I. Mc Culloch and M. D. McGehee, *Adv. Funct. Mater.*, **2009**, 19, 1173.

[23] Akshaya K.Palai, Hyejin Cho, Sungwoo Cho, Tae Joo Shin, Soonmin Jang, Seung-Un Park, Seungmoon Pyo, *Organic Electronics*, **2013**, 14, 5, 1396-1406.

초 록

유기 전계 효과 트랜지스터를 위한 1,5-Naphthyridine-2,6-dione (NTD) 유도체의 구조 – 성질에 관한 연구

리우메이린

공과대학 재료공학부

서울대학교 대학원

유기 전계 효과 트랜지스터(OFETs)는 유연성 및 용액 공정성의 이점 때문에 주목을 받고있다. 유기 트랜지스터의 장점을 살펴보면 공정이 쉽고 저비용제작이 가능하며, 가벼우면서도 좋은 유연성을 가진다는 장점을 가지고 있어서센서, 메모리, 디스플레이 백플레인 등에 다양하게 적용하고 있다. 최근, 연구자들이 트랜지스터에 적용되는 물질 중에 락탐 작용기를 포함하는 물질들에 많은 관심은 갖고 있다. 락탐 작용기를 포함하는 물질들은 독특한 전자-당김 효과에 의한 높은 전자 친화력을 가지게 되어서 LUMO 레벨이 더 안정화될 수 있고, N-원자 위치에 용해성이 있는 사슬을 도입해서 용해도를 조절하는 것도 가능하다. 또한, 평평한 구조에 기인한 강한 파이-파이 상호작용이 있어서 좋은 전자-받개 빌딩 블록으로 많은 연구를 진행하고 있다. 그중에 가장 대표적인 소재는 디케토피롤로피롤(DPP)로써 많이 연구되고 있지만, DPP

는 평면성이 부족하기 때문에 트랜지스터의 성능을 더 향상시키기 어려운 문제가 있다.

　　최근 새로운 전자-받개 비스-락탐 기반의 빌딩 블록인 3,7-dithiophen-2-yl-1,5-dialkyl-1,5-naphthyridine-2,6-dione(NTDT)이 성공적으로 개발된 바 있다. 잘 알려져 있고 많이 쓰이는 비스-락탐 구조인 2,5-dioctyl-3,6-di(thiophen-2-yl)pyrrolo[3,4-c]pyrrole-1,4-dione(DPPT)와 달리, NTDT는 이차원 분자간 상호 작용 (2D) CH⋯O = C이 있으며, 평면성이 높은 분자 구조 및 강한 분자간 π-π 스태킹으로 인한 층상구조와 높은 전자이동도, 높은 결정성을 가지므로 유기 전계-효과 트랜지스터로의 소자 적용이 유리하다. 그러나 NTDT가 트랜지스터 소자에서 괜찮은 이동도를 보여 주었지만 여전히 개선의 여지는 많이 남아있으며, 이를 위해 NTDT 유도체에 대한 구조-물성 상관관계에 대한 연구가 필요한 상황이다.

　　본 연구에서는 주로 NTDT 유도체의 평면성와 결정성이 OFET 소자의 성능에 미치는 효과를 탐구하였다. 우리는 NTDT 양쪽에 티오펜고리의 다른 위치에 헥실 사슬을 도입해서 NTDT 유도체를 디자인하고 합성했다. 광학적, 전기화학적 특성은 자외선-가시광선 분광법, 발광 분광법 및 순환 전압 전류(CV)을 통해 측정하였고, 밀도범함수 이론 (DFT)을 사용하여 이론적인 에너지 레벨을 계산해서 연구하였다. 헥실기의 치환 위치에 따라서 NTDT 유도체의 분자 평탄도에 영향을 미치므로 광전자 및 열적 특성이 다른 것을 확인하였다. 또한 형광사진을 보면 알킬기의 치환에 관계없이 용액에서의 형광 효율은 모두 100%정도로 높고 균일하게 나온 반면 고체 상태 필름의 경우 hexyl기의 치환 위치에 따라 상이한 ΦPL 값을 가지고 있는 것을 확인할 수가 있습니다. 합성된 물질을 이용해서 유기전계효과 트랜지스터의 성능을 측정한 결과을 보면 다 p형 소자의 특성이 나타나고 온도를 조절한 후에 Octyl_NTDT_αhexyl이 70도에서 최대 정공이동도이 0.44 cm^2 V^{-1} s^{-1}을 보여 주었다,또한 NTD가 분자간 상호작용이 커서 용해도 낮은 문제가 있기 때문에 본연구에서 알킬 사슬을 도입해서 용액공정용 트랜지스터을 측정해봤고 최대

정공이동도 9.11×10^{-2} cm^2 V^{-1} s^{-1}을 보여주었다. 따라서, 진공증착 및 용액공정으로 제작한 OFET 장치에서 NTDT 유도체의 헥실기 치환 위치와 소자 성능 간에 상관 관계가 있음을 확인하였다.

주요어: 디케토피롤로피롤, 단분자,구조특성관계, 유기저계효과 트랜지스터